Published OnlineFirst April 11, 2014; DOI: 10.1158/1078-0432.CCR-13-3169

Acquisition of data (provided animals, acquired and managed patients, provided facilities, etc.): S. Kobayashi, E. Watanabe, K. Yuji, N. Oyaizu, S. Asanuma, A. Tojo
Analysis and interpretation of data (e.g., statistical analysis, biostatistics, computational analysis): S. Kobayashi, K. Nakano, T. Ishigaki, N. Oyaizu, M. Yamagishi, T. Watanabe
Writing, review, and/or revision of the manuscript: S. Kobayashi, K. Nakano, A. Tojo, T. Watanabe, K. Uchimaru
Administrative, technical, or material support (i.e., reporting or organizing data, constructing databases): T. Ishigaki, N. Ohno, N. Watanabe
Study supervision: A. Tojo, T. Watanabe, K. Uchimaru

Acknowledgments

The authors thank Drs. Kazunari Yamaguchi (National Institute of Infectious Diseases, Tokyo, Japan) and Yoshinori Murakami (the University of Tokyo) for their constructive comments; Yuji Zaike (Clinical Laboratory, Research Hospital, Institute of Medical Science, the University of Tokyo) for his excellent technical advice; Keisuke Takahashi, Sanae Suzuki, and members of our laboratory for assistance; and the hospital staff, which has made a commitment to providing high-quality care to all patients. The English in this document has been checked by at least two professional editors, both native speakers of English.

Grant Support

This work was supported by grants-in-aid for scientific research awarded to K. Uchimaru (no. 22591028) and T. Watanabe (no. 23390250) by the Ministry of Education, Culture, Sports, Science and Technology of Japan.

The costs of publication of this article were defrayed in part by the payment of page charges. This article must therefore be hereby marked *advertisement* in accordance with 18 U.S.C. Section 1734 solely to indicate this fact.

Received November 19, 2013; revised March 19, 2014; accepted March 26, 2014; published OnlineFirst April 11, 2014.

References

1. Yoshida M, Miyoshi I, Hinuma Y. Isolation and characterization of retrovirus from cell lines of human adult T-cell leukemia and its implication in the disease. Proc Natl Acad Sci U S A 1982;79:2031–5.
2. Osame M, Usuku K, Izumo S, Ijichi N, Amitani H, Igata A, et al. HTLV-I associated myelopathy, a new clinical entity. Lancet 1986;1:1031–2.
3. Mochizuki M, Watanabe T, Yamaguchi K, Takatsuki K, Yoshimura K, Shirao M, et al. HTLV-I uveitis: a distinct clinical entity caused by HTLV-I. Jpn J Cancer Res 1992;83:236–9.
4. Yamaguchi K, Watanabe T. Human T lymphotropic virus type-I and adult T-cell leukemia in Japan. Int J Hematol 2002;76 Suppl 2:240–5.
5. Murphy EL, Hanchard B, Figueroa JP, Gibbs WN, Lofters WS, Campbell M, et al. Modelling the risk of adult T-cell leukemia/lymphoma in persons infected with human T-lymphotropic virus type I. Int J Cancer 1989;43:250–3.
6. Iwanaga M, Watanabe T, Yamaguchi K. Adult T-cell leukemia: a review of epidemiological evidence. Front Microbiol 2012;3:322.
7. Okamoto T, Ohno Y, Tsugane S, Watanabe S, Shimoyama M, Tajima K, et al. Multi-step carcinogenesis model for adult T-cell leukemia. Jpn J Cancer Res 1989;80:191–5.
8. Matsuoka M, Jeang KT. Human T-cell leukemia virus type 1 (HTLV-1) and leukemic transformation: viral infectivity, Tax, HBZ and therapy. Oncogene 2011;30:1379–89.
9. Matsuoka M, Jeang KT. Human T-cell leukaemia virus type 1 (HTLV-1) infectivity and cellular transformation. Nat Rev Cancer 2007;7:270–80.
10. Yoshida M. Molecular approach to human leukemia: isolation and characterization of the first human retrovirus HTLV-1 and its impact on tumorigenesis in adult T-cell leukemia. Proc Jpn Acad Ser B Phys Biol Sci 2010;86:117–30.
11. Yamagishi M, Watanabe T. Molecular hallmarks of adult T cell leukemia. Front Microbiol 2012;3:334.
12. Tsukasaki K, Hermine O, Bazarbachi A, Ratner L, Ramos JC, Harrington W Jr, et al. Definition, prognostic factors, treatment, and response criteria of adult T-cell leukemia-lymphoma: a proposal from an international consensus meeting. J Clin Oncol 2009;27:453–9.
13. Ishida T, Joh T, Uike N, Yamamoto K, Utsunomiya A, Yoshida S, et al. Defucosylated anti-CCR4 monoclonal antibody (KW-0761) for relapsed adult T-cell leukemia-lymphoma: a multicenter phase II study. J Clin Oncol 2012;30:837–42.
14. Tian Y, Kobayashi S, Ohno N, Isobe M, Tsuda M, Zaike Y, et al. Leukemic T cells are specifically enriched in a unique CD3(dim) CD7(low) subpopulation of CD4(+) T cells in acute-type adult T-cell leukemia. Cancer Sci 2011;102:569–77.
15. Kobayashi S, Tian Y, Ohno N, Yuji K, Ishigaki T, Isobe M, et al. The CD3 versus CD7 Plot in Multicolor Flow Cytometry Reflects Progression of Disease Stage in Patients Infected with HTLV-I. PLoS One 2013;8:e53728.
16. Reinhold U, Abken H. CD4+ CD7- T cells: a separate subpopulation of memory T cells? J Clin Immunol 1997;17:265–71.
17. Reinhold U, Abken H, Kukel S, Moll M, Muller R, Oltermann I, et al. CD7- T cells represent a subset of normal human blood lymphocytes. J Immunol 1993;150:2081–9.
18. Leblond V, Othman TB, Blanc C, Theodorou I, Choquet S, Sutton L, et al. Expansion of CD4+CD7- T cells, a memory subset with preferential interleukin-4 production, after bone marrow transplantation. Transplantation 1997;64:1453–9.
19. Aandahl EM, Quigley MF, Moretto WJ, Moll M, Gonzalez VD, Sonnerborg A, et al. Expansion of CD7(low) and CD7(negative) CD8 T-cell effector subsets in HIV-1 infection: correlation with antigenic load and reversion by antiretroviral treatment. Blood 2004;104:3672–8.
20. Autran B, Legac E, Blanc C, Debre P. A Th0/Th2-like function of CD4+CD7- T helper cells from normal donors and HIV-infected patients. J Immunol 1995;154:1408–17.
21. Legac E, Autran B, Merle-Beral H, Katlama C, Debre P. CD4+CD7-CD57+ T cells: a new T-lymphocyte subset expanded during human immunodeficiency virus infection. Blood 1992;79:1746–53.
22. Schmidt D, Goronzy JJ, Weyand CM. CD4+ CD7- CD28- T cells are expanded in rheumatoid arthritis and are characterized by autoreactivity. J Clin Invest 1996;97:2027–37.
23. Willard-Gallo KE, Van de Keere F, Kettmann R. A specific defect in CD3 gamma-chain gene transcription results in loss of T-cell receptor/CD3 expression late after human immunodeficiency virus infection of a CD4+ T-cell line. Proc Natl Acad Sci U S A 1990;87:6713–7.
24. Sasaki H, Nishikata I, Shiraga T, Akamatsu E, Fukami T, Hidaka T, et al. Overexpression of a cell adhesion molecule, TSLC1, as a possible molecular marker for acute-type adult T-cell leukemia. Blood 2005;105:1204–13.
25. Nakahata S, Morishita K. CADM1/TSLC1 is a novel cell surface marker for adult T-cell leukemia/lymphoma. J Clin Exp Hematop 2012;52:17–22.
26. Kuramochi M, Fukuhara H, Nobukuni T, Kanbe T, Maruyama T, Ghosh HP, et al. TSLC1 is a tumor-suppressor gene in human non-small-cell lung cancer. Nat Genet 2001;27:427–30.
27. Nakahata S, Saito Y, Marutsuka K, Hidaka T, Maeda K, Hatakeyama K, et al. Clinical significance of CADM1/TSLC1/IgSF4 expression in adult T-cell leukemia/lymphoma. Leukemia 2012;26:1238–46.
28. Sugamura K, Fujii M, Kannagi M, Sakitani M, Takeuchi M, Hinuma Y. Cell surface phenotypes and expression of viral antigens of various human cell lines carrying human T-cell leukemia virus. Int J Cancer 1984;34:221–8.
29. Shimoyama M. Diagnostic criteria and classification of clinical subtypes of adult T-cell leukaemia-lymphoma. A report from the Lymphoma Study Group (1984–87). Br J Haematol 1991;79:428–37.
30. Iwanaga M, Watanabe T, Utsunomiya A, Okayama A, Uchimaru K, Koh KR, et al. Human T-cell leukemia virus type I (HTLV-1) proviral load and

Published OnlineFirst April 11, 2014; DOI: 10.1158/1078-0432.CCR-13-3169

disease progression in asymptomatic HTLV-1 carriers: a nationwide prospective study in Japan. Blood 2010;116:1211–9.

31. Yamagishi M, Nakano K, Miyake A, Yamochi T, Kagami Y, Tsutsumi A, et al. Polycomb-mediated loss of miR-31 activates NIK-dependent NF-kappaB pathway in adult T cell leukemia and other cancers. Cancer Cell 2012;21:121–35.
32. Asanuma S, Yamagishi M, Kawanami K, Nakano K, Sato-Otsubo A, Muto S, et al. Adult T-cell leukemia cells are characterized by abnormalities of Helios expression that promote T-cell growth. Cancer Sci 2013;104:1097–106.
33. Yamaguchi K, Kiyokawa T, Nakada K, Yul LS, Asou N, Ishii T, et al. Polyclonal integration of HTLV-I proviral DNA in lymphocytes from HTLV-I seropositive individuals: an intermediate state between the healthy carrier state and smouldering ATL. Br J Haematol 1988;68: 169–74.
34. Kamihira S, Iwanaga M, Doi Y, Sasaki D, Mori S, Tsurda K, et al. Heterogeneity in clonal nature in the smoldering subtype of adult T-cell leukemia: continuity from carrier status to smoldering ATL. Int J Hematol 2012;95:399–408.
35. Masuda M, Maruyama T, Ohta T, Ito A, Hayashi T, Tsukasaki K, et al. CADM1 interacts with Tiam1 and promotes invasive phenotype of human T-cell leukemia virus type I-transformed cells and adult T-cell leukemia cells. J Biol Chem 2010;285: 15511–22.

Cancer Science
Japanese Cancer Association JCA
Open Access

Epigenetic deregulation of *Ellis Van Creveld* confers robust Hedgehog signaling in adult T-cell leukemia

Ryutaro Takahashi,[1,6] Makoto Yamagishi,[1,6] Kazumi Nakano,[1] Toshiko Yamochi,[2] Tadanori Yamochi,[1] Dai Fujikawa,[1] Makoto Nakashima,[1] Yuetsu Tanaka,[3] Kaoru Uchimaru,[4] Atae Utsunomiya[5] and Toshiki Watanabe[1]

[1]Graduate School of Frontier Sciences, The University of Tokyo, Tokyo; [2]Department of Pathology, Showa University School of Medicine, Tokyo; [3]Department of Immunology, Graduate School of Medicine, University of the Ryukyus, Okinawa; [4]Institute of Medical Science, The University of Tokyo, Tokyo; [5]Department of Hematology, Imamura Bun-in Hospital, Kagoshima, Japan

Key words

ATL, epigenetics, EVC, Hedgehog, HTLV-1

Correspondence

Toshiki Watanabe, Laboratory of Tumor Cell Biology, Department of Medical Genome Sciences, Graduate School of Frontier Sciences, The University of Tokyo, 4-6-1 Shirokanedai, Minato-ku, Tokyo 108-8639, Japan.
Tel: +81-3-5449-5298; Fax: +81-3-5449-5418;
E-mail: tnabe@ims.u-tokyo.ac.jp

[6]These authors contributed equally to this study.

Funding information

JSPS KAKENHI (24790436). (23390250). MEXT KAKENHI (221S0001). Ministry of Health, Labour and Welfare H24-Third Term Cancer-004 Uehara Memorial Foundation.

Received April 14, 2014; Revised June 20, 2014; Accepted July 1, 2014

Cancer Sci **105** (2014) 1160–1169

doi: 10.1111/cas.12480

One of the hallmarks of cancer, global gene expression alteration, is closely associated with the development and malignant characteristics associated with adult T-cell leukemia (ATL) as well as other cancers. Here, we show that aberrant overexpression of the *Ellis Van Creveld* (EVC) family is responsible for cellular Hedgehog (HH) activation, which provides the pro-survival ability of ATL cells. Using microarray, quantitative RT-PCR and immunohistochemistry we have demonstrated that EVC is significantly upregulated in ATL and human T-cell leukemia virus type I (HTLV-1)-infected cells. Epigenetic marks, including histone H3 acetylation and Lys4 trimethylation, are specifically accumulated at the *EVC* locus in ATL samples. The HTLV-1 Tax participates in the coordination of EVC expression in an epigenetic fashion. The treatment of shRNA targeting EVC, as well as the transcription factors for HH signaling, diminishes the HH activation and leads to apoptotic death in ATL cell lines. We also showed that a HH signaling inhibitor, GANT61, induces strong apoptosis in the established ATL cell lines and patient-derived primary ATL cells. Therefore, our data indicate that HH activation is involved in the regulation of leukemic cell survival. The epigenetically deregulated EVC appears to play an important role for HH activation. The possible use of EVC as a specific cell marker and a novel drug target for HTLV-1-infected T-cells is implicated by these findings. The HH inhibitors are suggested as drug candidates for ATL therapy. Our findings also suggest chromatin rearrangement associated with active histone markers in ATL.

Adult T-cell leukemia (ATL) is a malignant T-cell disorder caused by infection with a human retrovirus, human T-cell leukemia virus type I (HTLV-1).[1–3] The prognosis of aggressive types of ATL is poor.[4] At present, ATL is an intractable disease in human beings. To prevent the development of ATL and the poor prognosis that is associated with it, the development of effective therapies based on the molecular characteristics is needed.

To explore effective drugs, precise understanding of the molecular mechanism of ATL pathogenesis is essential. We have previously reported that genetic and epigenetic imbalances and following aberrant gene expressions are the main framework for ATL tumor cells.[5,6] In addition, the involvement of systemic downregulation of cellular microRNA has been implicated in the leukemogenesis of ATL. So far, several host cellular signaling abnormalities induced by HTLV-1 Tax in the early phase of infection[6–8] and the aberrant activation of nuclear factor-kappa B (NF-κB) contribute to ATL leukemogenesis.[9,10] Although other several molecular deregulations have been suggested in ATL, we have not completely covered the landscape of signaling networks in ATL.

Recently, Hedgehog (HH) signaling has been reported as an oncogenic pathway in many types of cancers.[11,12] Constitutive HH activation leads to the overproliferation or survival of several cancer cells, such as basal cell carcinoma or B-cell lymphomas.[13–15] There are some HH inhibitors under clinical trial as drug candidates against those cancers.[16]

In the present study, using ATL patient samples and some ATL models, we found two specific gene overproductions in ATL, *Ellis Van Creveld syndrome 1* (*EVC1*) and *EVC2*, which belong to the EVC family of genes that are implicated in HH regulation.[17–19] We demonstrated that epigenetically upregulated EVC was associated with cellular HH activity. *EVC* and other regulatory factors for HH signaling were responsible for the survival of ATL cell lines and also primary ATL samples. Direct evidence from the ATL samples revealed that universal epigenetic marks associated with actively transcribed genes were rearranged in the leukemic cells. These findings may shed light on the abnormal gene expression signature and leukemic cell traits observed in ATL.

Materials and Methods

Patient samples. The primary peripheral blood mononuclear cells (PBMC) from ATL patients and healthy volunteers were a part of those collected with informed consent as a collaborative project of the Joint Study on Prognostic Factors of ATL Development (JSPFAD). The project was approved by the University

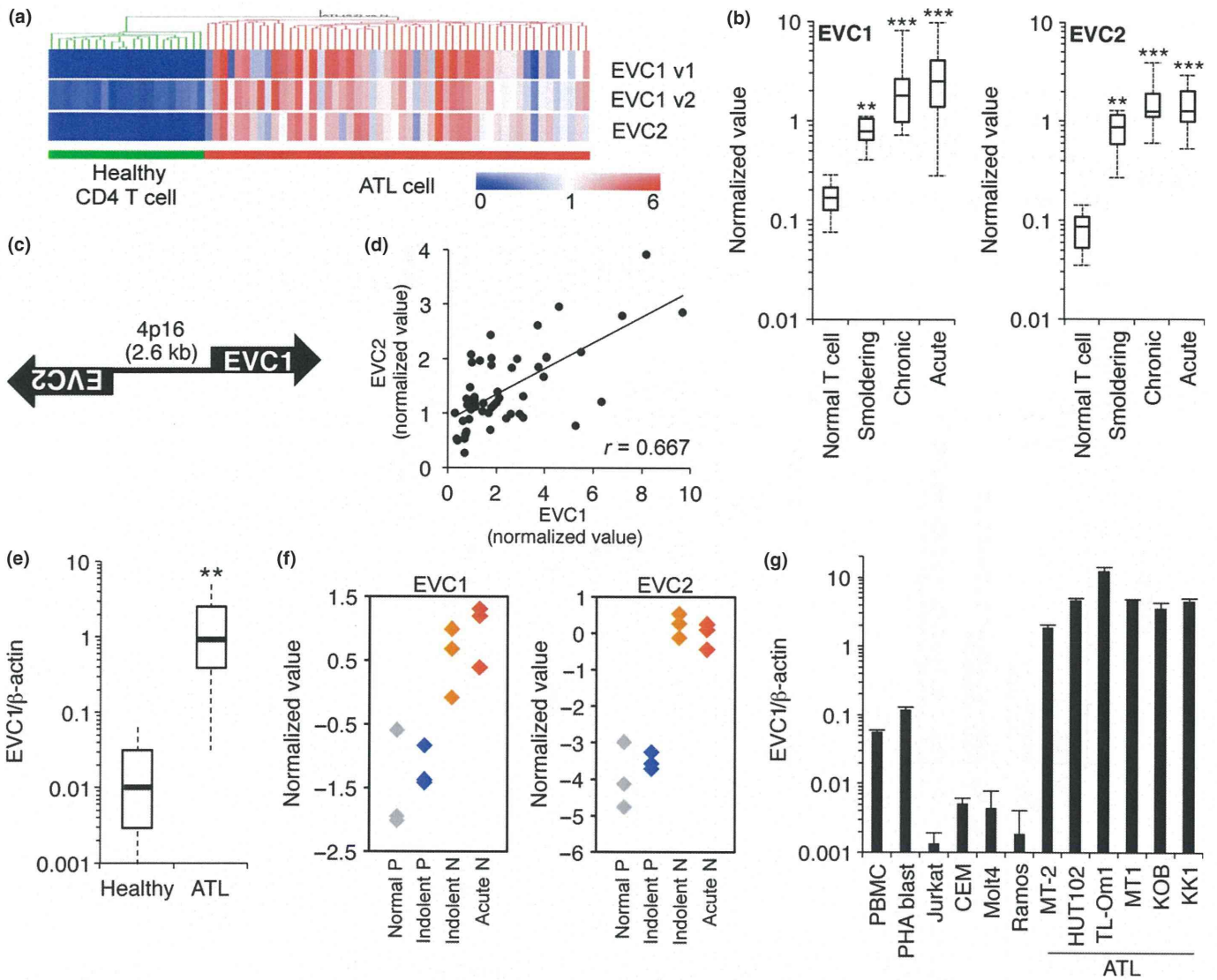

Fig. 1. *EVC* overexpression in ATL. (a, b) Microarray heatmap (a) and box plot (b) of *EVC*. $^{**}P < 0.01$. $^{***}P < 0.001$. (c) Schematic illustration of locus encoding *EVC1/2*. (d) Individual expression values ($n = 52$) between *EVC1* and *EVC2*. (e) *EVC1* mRNA level in ATL patient PBMC (total, $n = 11$; acute, $n = 7$; chronic, $n = 4$) and in CD4+ T cells from healthy donors ($n = 6$) evaluated using quantitative RT-PCR (qRT-PCR). $^{**}P < 0.01$. (f) *EVC1* and *EVC2* levels in CADM1 versus CD7 plot subpopulations. Normal P, CD4+/CADM1−/CD7+ T cells from healthy donors; Indolent P, CD4+/CADM1−/CD7+ from indolent ATL patients; Indolent N, CD4+/CADM1+/CD7− from indolent ATL patients; Acute N, CD4+/CADM1+/CD7− from acute ATL patients. The gene expression microarray dataset is available in Kobayashi *et al.*[25] (g) *EVC1* levels in various cell lines examined using qRT-PCR ($n = 3$, mean ± SD).

of Tokyo and Showa University research ethics committees. The PBMC were isolated using Ficoll separation and maintained in RPMI1640 (Invitrogen, Carlsbad, CA, USA) supplemented with 1% of self-serum and antibiotics (Invitrogen). Clinical information is shown in the Supporting Information Methods.

Microarray analysis. Gene expression profiling of ATL patient samples and normal CD4+ T cells has been performed previously.[5] The coordinate has been deposited in the Gene Expression Omnibus database (GSE33615).

Cell culture. The HTLV-1-infected cell lines MT-2 and HUT102, ATL-derived cells MT-1 and TL-Om1, and other leukemic cell lines were cultured in RPMI1640 with 10% FCS. ATL-derived KOB and KK1 were cultured in RPMI1640 with 10% FCS and 10 ng/mL recombinant human IL-2 (R&D Systems, Minneapolis, MN, USA). The 293T cell was cultured in DMEM with 10% FCS. All cell lines were cultured at 37°C, with 5% CO_2.

Plasmids and HH activity analysis. Tax-encoding plasmids have been described previously.[20] *EVC1* cDNA was amplified as two fragments from the human cDNA library. Cellular HH activity was evaluated using a dual-luciferase assay (Promega, Madison, WI, USA).[21] Briefly, 7 × GLI binding site (GACACCCA)-luciferase plasmid and control RSV-Renilla plasmid were co-transfected into target cells using Lipofectamine2000 (Invitrogen). At 24 h post-transfection, the cells were collected and analyzed using a dual-luciferase assay.

Quantitative RT-PCR. Procedures for RNA isolation and RT-PCR have been described previously.[5] Primer sets for quantitative RT-PCR (qRT-PCR) are provided in the Supporting Information Methods.

Epigenetic analyses. Bisulfite treatment was conducted using a MethylEasy Xceed Rapid DNA Bisulphite Modification kit (Human Genetic Signatures, NSW, Australia). For evaluating histone covalent modifications, a chromatin immunoprecipita-

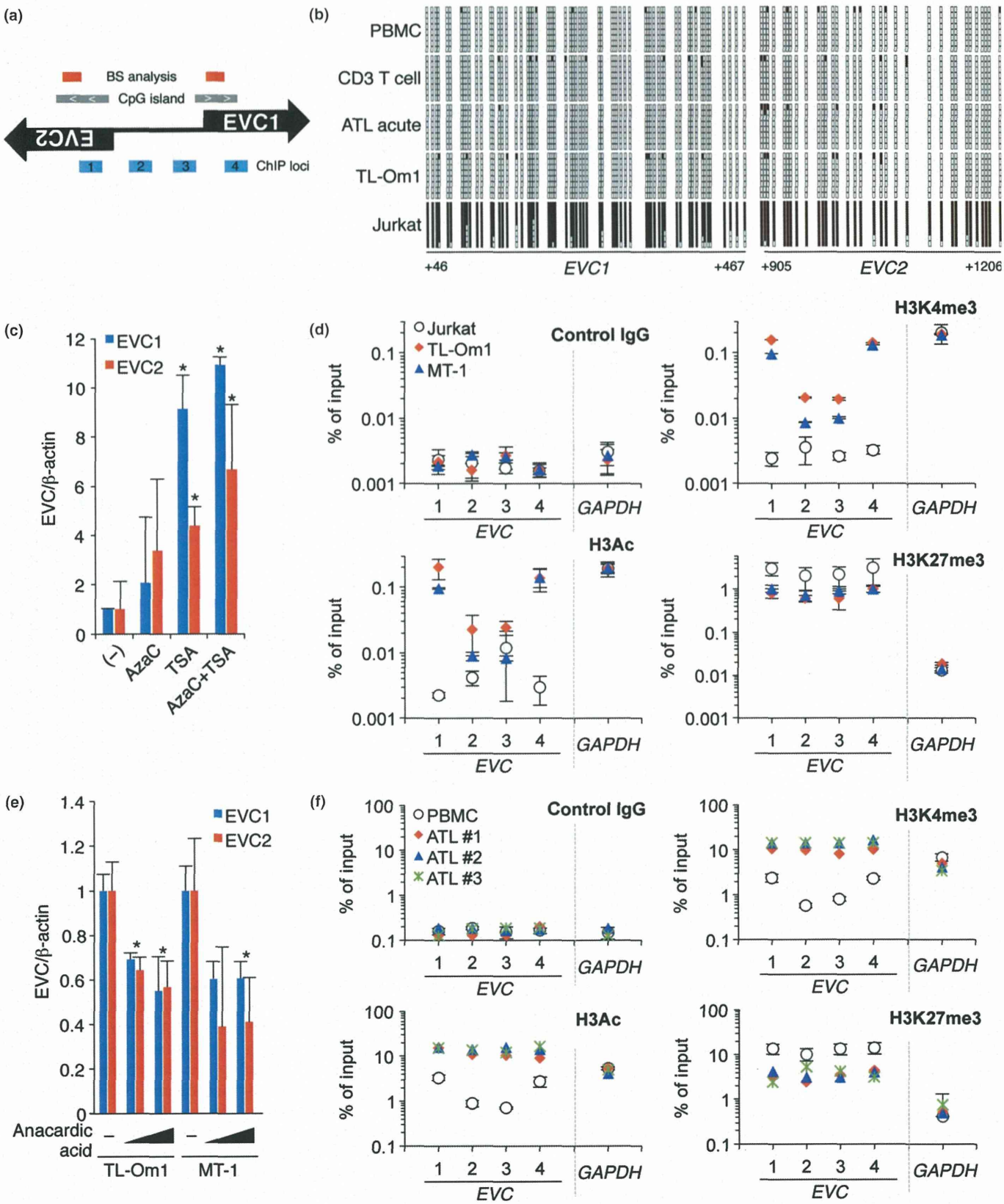

Fig. 2. Epigenetic reprogramming in the *EVC* locus. (a) Schematic of CpG islands and chromatin immunoprecipitation (ChIP) loci. (b) Results of bisulfite sequencing (+46 to +466 from *EVC1* transcription start site [TSS]; +905 to +1206 from *EVC2* TSS). The black and empty boxes represent methylated and unmethylated CpG, respectively. (c) *EVC* RNA levels in Jurkat cells in the presence or absence of epigenetic drugs ($n = 3$, mean ± SD). *$P < 0.05$. (d) Histone covalent modifications at *EVC* and *GAPDH* loci in three cell lines were analyzed using PCR-based ChIP assay with specific antibodies. Positions of primer sets for the real-time PCR are indicated in (a). Enrichment values relative to input samples are plotted. (e) TL-Om1 and MT-1 cells were treated with 1 or 5 μM of anacardic acid for 48 h and the *EVC* mRNA level was then analyzed ($n = 3$, mean ± SD). *$P < 0.05$. (f) Epigenetic changes in primary ATL samples. Three independent clinical samples were compared with normal PBMC ($n = 3$, mean ± SD).

tion (ChIP) assay was conducted as described previously.[5,22] Anti-H3K4me3 (#9751S; Cell Signaling, Danvers, MA, USA), anti-AcH3 (#06-599; Millipore, Billerica, MA, USA), anti-H3K27me3 (#39155; Active Motif, Carlsbad, CA, USA) and control IgG (I5381; SIGMA, St. Louis, MO, USA) were used for ChIP. Primers for the qPCR are provided in the Supporting Information Methods.

Immunohistochemistry. For preparation of the paraffin block of 293T cells, the cells were fixed in 20% of formalin/PBS for 24 h. After removing the formalin, alcohol dehydration and paraffin permeation were done using Tissue-Tek VIP5Jr (Sakura, Alphen aan den Rijn, The Netherlands). Paraffin blocks were sectioned at 3-μm thickness. The sections were then transferred to coating slide glasses (Muto pure chemicals, Bunkyo-ku, Tokyo, Japan). After paraffin removal, the paraffin sections of the 293T and ATL cells were treated with 3% H_2O_2. Antigen-retrieval treatment was done using Histofine antigen retrieval solution pH9 (Nichirei, Chuo-Ku, Tokyo, Japan) for 20 min under microwave radiation. After reaction with the first antibody, anti-EVC antibody (HPA008703, 1:400; SIGMA), and the second antibody (K5027, ENVISION Kit/HRP [DAB]; Dako, Bunkyo-ku, Tokyo, Japan), the sections were colored using ENVISION Kit/HRP [DAB] DAB+ (K3468; DAKO). Finally, the sections were stained with hematoxylin.

Lentivirus construction and production. Detailed procedures for lentivirus production have been described previously.[5] Briefly, replication-defective, self-inactivating lentivirus vectors were used.[23,24] shRNA were cloned into a CS-H1-EVBsd. High-titer viral solutions prepared using a centrifugation-based concentration were transduced into ATL cell lines using the spinoculation method. The transduced cells were

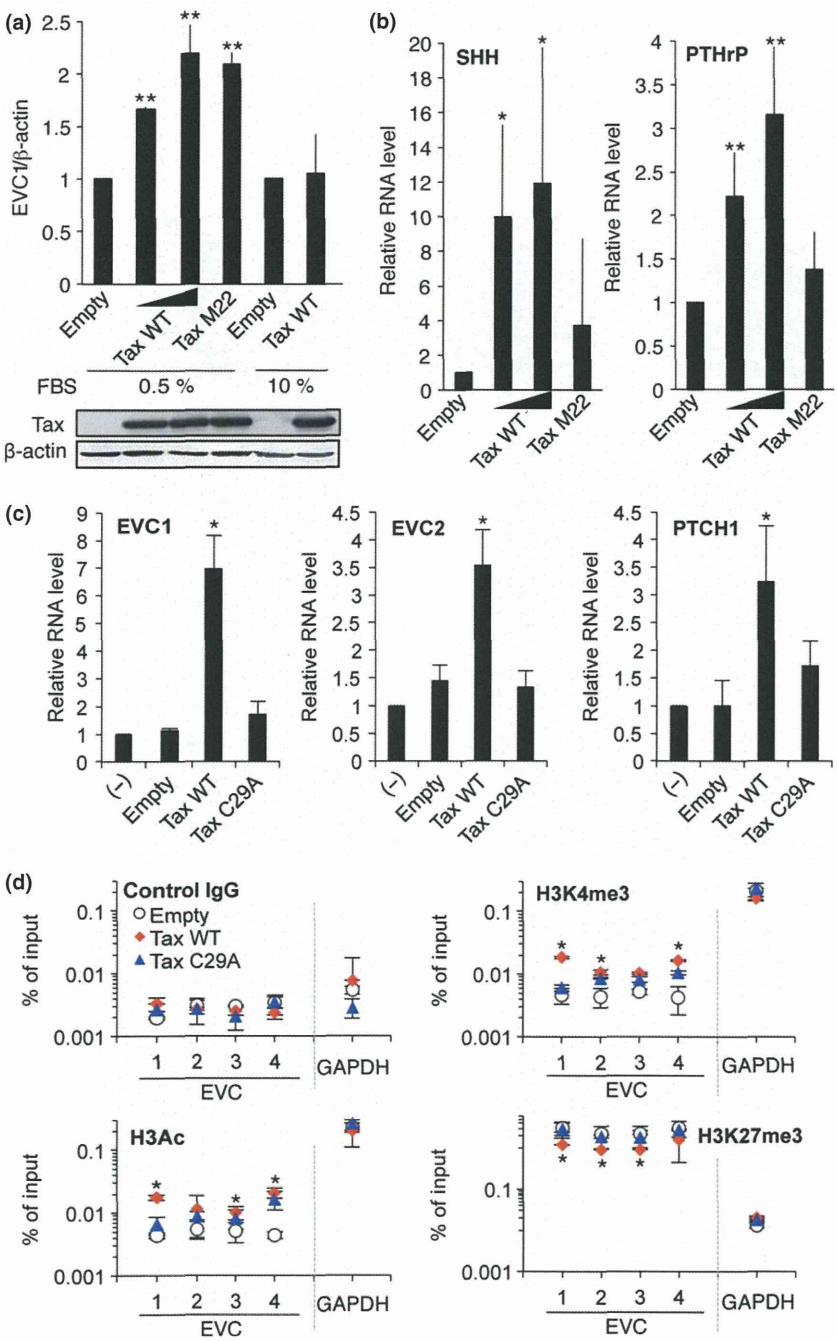

Fig. 3. Role of Tax in *EVC* regulation. (a) *EVC1* RNA levels are affected by Tax. The 293T cells in different FBS condition were transfected with the indicated plasmids. Relative *EVC1* levels were evaluated using quantitative RT-PCR (qRT-PCR) (top panel, $n = 3$, mean ± SD). $^{**}P < 0.01$. Tax expression was confir-med using western blotting with an anti-Tax antibody (Lt-4) (bottom panel). (b) Levels of *SHH* and *PTHrP* in the presence or absence of Tax ($n = 3$, mean ± SD). $^{*}P < 0.05$. $^{**}P < 0.01$. (c) *EVC* and *PTCH1* levels in Jurkat cells expressing Tax ($n = 3$, mean ± SD). $^{*}P < 0.05$. (d) Tax-mediated epigenetic changes. Histone modifications at *EVC* and *GAPDH* loci in Tax-expressing Jurkat cells were analyzed using a ChIP assay. $^{*}P < 0.05$ (Tax WT *vs* Empty). Primer positions are shown in Figure 2(a).

further selected by blastcidin and used within 14 days. shRNA sequences are described in the Supporting Information Methods.

Cell viability and apoptosis analyses. For the cell proliferation assay, 5000 cells were plated in a 96-well flat bottom plate with RPMI1640 medium supplemented with 1% FCS. After 1–3 days culture, cell numbers were evaluated using Cell Counting kit-8 (Dojindo, Kumamoto, Japan). The apoptosis cell was determined using PE Annexin V/7-AAD stainings (BD Pharmingen, San Jose, CA, USA). Detection of apoptotic cells was performed using FACSCalibur (Becton, Dickinson, Franklin Lakes, NJ, USA). Primary ATL cells were defined using sequential gating based on a Forward scatter/Side Scatter (FSC/SSC) pattern and a CD4-positive population (anti-CD4-FITC; BD Pharmingen). Collected data were analyzed using FlowJo software (Tree Star, Ashland, OR, USA).

Results

Epigenetic abnormalities in *EVC* regulation in ATL. We have determined the gene expression signature of ATL tumor cells by conducting massive microarrays.[5] The gene expression profiles from 52 ATL patients and 21 healthy donors identified a large number of specific gene upregulations in ATL cells. Among these, the genes encoding EVC1 and EVC2 were strikingly overexpressed in ATL patient samples, which had a relationship to disease progression (Fig. 1a,b). These genes are located in an identical chromosome *4p16*, under a bi-directional promoter (Fig. 1c), and their expressions have shown a strong positive correlation (Fig. 1d). The qRT-PCR revealed that the median of the *EVC1* mRNA level in ATL was 90.9-fold higher than that of normal CD4+ T-cells (Fig. 1e). Specificity of tumor-associated EVC expression was confirmed using the dataset from CADM1 versus CD7 plot subpopulation samples.[25] CADM1 expression and CD7 loss have recently been identified as highly sensitive molecular markers of HTLV-1-infected cells. *EVC1* and *EVC2* were significantly expressed in the CADM1+/CD7− tumorous population (Fig. 1f). The HTLV-1-infected and ATL-derived cells showed higher levels of *EVC1* mRNA compared with those in other leukemia and lymphoma cell lines and those of healthy PBMC (Fig. 1g). The MT-2 and HUT102 cells, which highly express HTLV-1 genes, showed high *EVC1* mRNA levels similar to those in ATL-derived cells.

Looking at the tumor-associated epigenetic reprogramming that was frequently observed in ATL,[5,6] we analyzed the epigenetic status of the *EVC* locus to clarify the possible

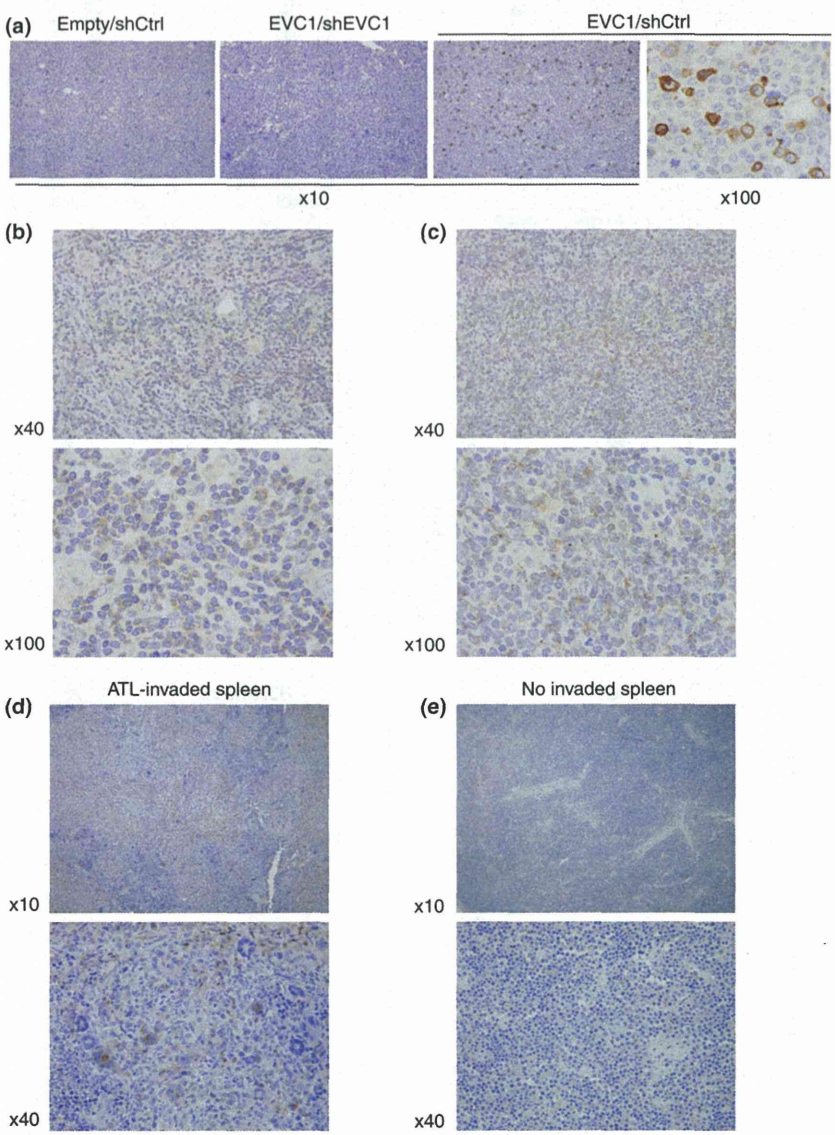

Fig. 4. EVC1 expression in ATL cells. (a–e) Immunohistochemistry-based EVC1 protein detection in paraffin-embedded samples: 293T transfected with the indicated plasmids (a), primary ATL lymph node (b, c, representative data are shown) and spleen from mice engrafted with primary ATL cells (d, tumor invasive, $n = 3$; e, non-invasive). These samples were stained with anti-EVC1 antibody and hematoxylin.

involvement of epigenetic variation in *EVC* deregulation. There were two typical CpG islands in the *EVC* locus whose transcription may be tightly regulated by the gain of CpG methylation (Fig. 2a). However, bisulfite sequencing revealed that DNA methylation was not acquired in normal lymphocytes, as well as in the primary ATL sample (Fig. 2b). CpG hypermethylation within the *EVC* locus was found only in Jurkat cells where the *EVC* expression was nearly undetectable (Fig. 1g). Instead, treatment with epigenetic drugs, particularly a histone deacetylase (HDAC) inhibitor tricostatin A (TSA), reactivated the *EVC* transcription in Jurkat cells, suggesting that histone modifications such as acetylation were involved in *EVC* regulation (Fig. 2c). To further address the epigenetic implication, we performed ChIP assays to assess the possible contribution of histone modification in *EVC* upregulation. The ATL cell lines showed significant accumulation (log-scale) of histone H3 acetylation (H3Ac) and H3K4 trimethylation (H3K4me3), which have been recognized generally as positive transcription marks around the transcription start site region of both *EVC1* and *EVC2* (Fig. 2d). Treatment with a pan-histone acetylase inhibitor, anacardic acid, reduced *EVC* transcription in ATL cell lines (Fig. 2e). Interestingly, H3K27me3, which has been implicated as a poor prognostic marker in ATL,[5,26] was decreased at the *EVC* locus in ATL cells. We confirmed directly the epigenetic reprogramming at the *EVC* locus in primary ATL samples (Fig. 2f). In summary, it appeared that the acquisition of active histone modifications and the reciprocal disappearance of H3K27me3 contributed to aberrant EVC transcription.

Role of HTLV-1 Tax in *EVC* transcription. Next we addressed whether Tax could participate in the deregulated *EVC1* transcription. Although Tax expression did not influence the *EVC1* mRNA levels in 293T cells at complete growth conditions, Tax activated *EVC1* transcription in a dose-dependent manner in serum-starved conditions (Fig. 3a). A NF-κB activation-defected Tax mutant, M22,[27] showed similar *EVC1* induction, suggesting that *EVC1* transcriptional activation was independent from NF-κB activation. Indeed, the pharmacological inhibition of NF-κB activity failed to prevent *EVC* transcription in ATL cell lines (data not shown). Meanwhile, Tax induced transcription of *Sonic hedgehog* (*Shh*), which encodes the HH activation ligand, in a NF-κB-dependent manner (Fig. 3b). The experimental condition was validated by the evaluation of *PTHrP*, which has been known to be a Tax and NF-κB-targeted gene. HTLV-1 *HBZ* did not affect *EVC* transcription (Supporting Information Fig. S1).

We examined the possible relationship between Tax and histone modifications. For this purpose, we established lentiviral vectors inducing stable Tax expression in Jurkat cells. More than 80% of transduction efficiencies were achieved in all tested cells. Tax induced transcription of *EVC1* and *EVC2*, as well as the HH target gene *PTCH1* (Fig. 3c). Interestingly, the Tax C29A mutant, which was unable to localize in the nucleus,[28] failed to induce *EVC*, suggesting that *EVC* induction was directly caused by the nuclear-localized Tax. A ChIP assay revealed that the Tax wild type, but not the C29A mutant, directly accumulated H3K4me3 and H3Ac in the *EVC* locus (Fig. 3d). Thus, Tax appeared to, at least partially, induce *EVC* expression through epigenetic reprogramming.

EVC1 expression in primary ATL cell. We performed immunohistochemistry (IHC) with a commercially available antibody that recognized EVC1. First, we stained paraffin-embedded 293T cells transduced with the EVC1-expressing plasmid to test the antibody specificity. Strong positivity was detected in the plasmid-transduced sample but not in samples with untreated or concomitantly treated with shRNA targeting *EVC1* (Fig. 4a). Using this antibody we investigated EVC1 expression in several aggressive ATL cases. Most ATL cases showed stable EVC1 positivity (7/8, 87.5%; two representatives in Fig. 4b,c). We noted that all EVC1-positive cells were dysplastic. Furthermore, EVC1 expression was clearly detected in a mouse ATL model that was established using xenotrans-

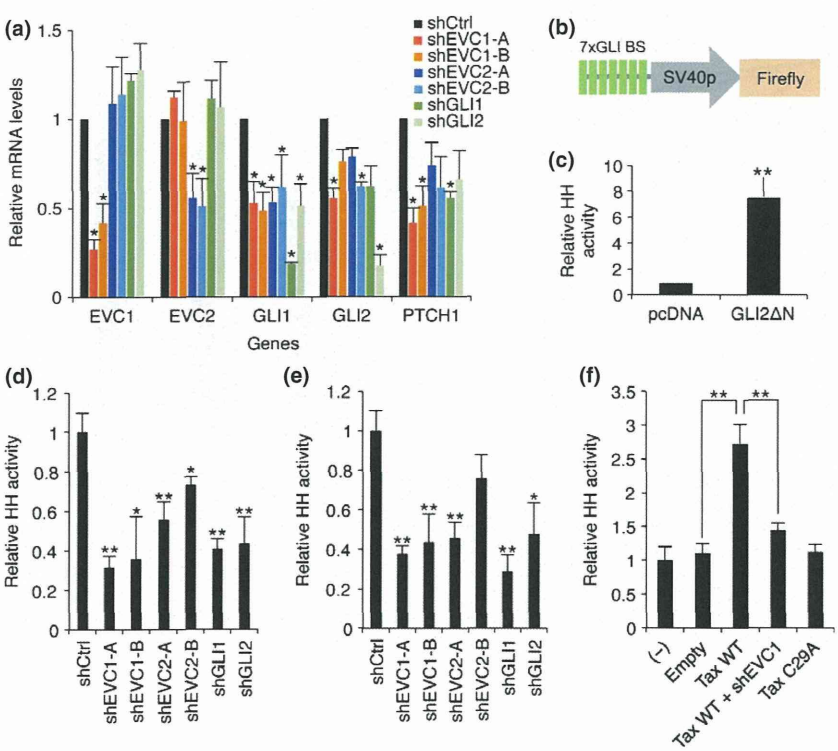

Fig. 5. EVC supports Hedgehog (HH) activity. (a) Relative RNA levels in shRNA-expressing TL-Om1 cells ($n = 3$, mean ± SD). $^*P < 0.05$. (b) Luciferase reporter plasmid containing 7 × sequential GLI-binding sites. (c) GLI2ΔN activa-ted HH activity ($n = 3$, mean ± SD). $^{**}P < 0.01$. (d–f) Hedgehog activity in various shRNA-expressing TL-Om1 (d), MT-2 (e) and Tax and shEVC1-expressing Jurkat (f) ($n = 3$~4, mean ± SD). $^*P < 0.05$. $^{**}P < 0.01$.

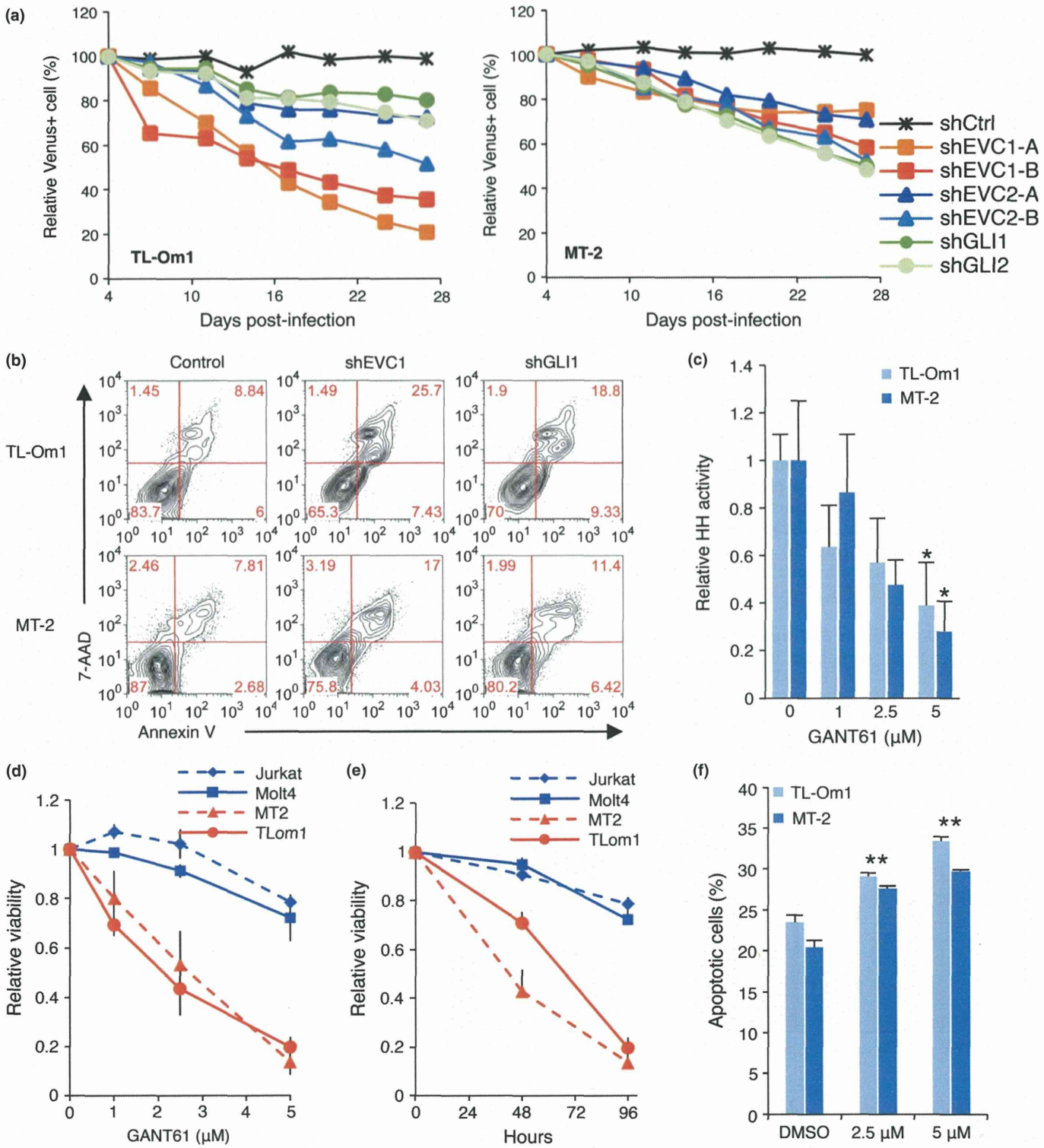

Fig. 6. Hedgehog (HH)-dependent ATL cell survival. (a) Time course of the abundance of Venus+ TL-Om1 (left) and MT-2 (right) infected with lentiviral vector expressing control shRNA (shCtrl), either of two shRNA targeting EVC1 and EVC2, or shRNA targeting GLI1 and GLI2, then cultured for 27 days together with uninfected cells. Data are representative of three independent experiments. Results are presented relative to those of cells at 4 days post-infection. (b) shRNA-mediated apoptosis induction. shRNA-expressing cells were cultured in 1% FBS for 72 h. The apoptotic pattern was defined by gating with Venus+ and Annexin V/7-AAD ($n = 3$, representative data). (c) GANT61 inhibited HH activity in ATL cells ($n = 3$, mean ± SD). $^*P < 0.05$. (d–e) GANT61 reduced ATL cell viability ($n = 3$, mean ± SD). The cells were treated with the indicated concentrations of GANT61 for 96 h (d) or with 5 μM of GANT61 for the indicated time periods (e). Cells were maintained in 1% FCS. (f) GANT61-dependent apoptosis analyzed using Annexin V/7-AAD staining ($n = 3$, mean ± SD). $^{**}P < 0.01$.

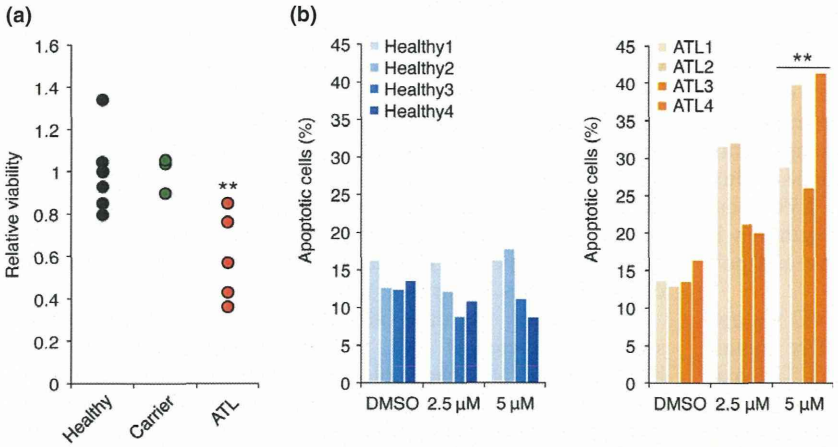

Fig. 7. GANT61 treatment reduced cell viabilities of primary ATL samples. (a) Effect of GANT61 in primary PBMC samples. The PBMC from healthy donors ($n = 7$), asymptomatic carriers ($n = 3$) and ATL patients ($n = 5$) were exposed in 5 μM of GANT61 for 72 h. Cells were maintained in media with 1% self-serum. $^{**}P < 0.01$. (b) GANT61-dependent apoptosis in ATL samples. The PBMC from healthy donors ($n = 4$) and ATL patients ($n = 4$) were treated with 5 μM of GANT61 for 72 h. Graphs show percentiles of apoptotic population in CD4+ cells $^{**}P < 0.01$.

plantation of primary tumor cells derived from an ATL patient. The lymphoma cells specifically expressed EVC1 (Fig. 4d,e). Taken together, EVC1 protein was definitely expressed in ATL cells.

EVC in HH activation. The EVC family has been implicated in HH signaling.[18,19] We performed the knockdown of EVC in TL-Om1 and MT-2 cells, which all highly expressed EVC (Fig. 1g). Specific knockdown was accomplished using lentivirus harboring specific and previously validated shRNA against EVC1, EVC2 or GLI transcription factors in the HH cascade. The qRT-PCR revealed the knockdown efficiency and also the HH activity as the RNA levels of *PTCH1* and *GLI1* were well-established HH activity markers.[29] The EVC depletion resulted in reduction of *PTCH1* and *GLI1* mRNA levels (Fig. 5a). Next we established a luciferase reporter containing 7 × sequential GLI-binding sites (Fig. 5b), which strongly responded against GLI2ΔN, a constitutive active form of GLI2[12] (Fig. 5c). As expected, the knockdown of EVC1 and EVC2 represented diminished HH activity in TL-Om1 and MT-2 cells (Fig. 5d,e). In addition, Tax activated the HH signal in Jurkat cells (Fig. 5f). Knockdown of EVC1 cancelled Tax-directed HH activation, suggesting that Tax affects HH signaling through, at least partially, EVC induction epigenetically.

EVC-dependent cell survival in ATL. Aberrant activation of HH provides cell survival ability in myeloma and lymphoma.[14,15] We found that different shRNA targeting EVC and GLI caused a progressive depletion of Venus+ cells (Fig. 6a). Knockdown of EVC1 or EVC2 attenuated ATL cell proliferation (Fig. S2). The growth defect was associated with a substantial decrease in the expression of targeted genes (Fig. 5). We then measured the apoptotic status by staining Annexin V/7-AAD. Specific analyses within the knocked down cells were achieved by gating with Venus fluorescence. At complete growth condition, slight but steady apoptosis was induced by EVC1 knockdown in MT-2 and TL-Om1 cells (data not shown). Furthermore, strong apoptosis was observed in EVC1-depleted cells at low FCS condition (Fig. 6b). This cell death appeared to be due to HH inactivation because GLI1-knocked down cells showed similar results.

Specific killing of ATL cell by GANT61. GANT61 is a cell-permeable hexahydropyrimidine compound, which has been shown to be a well-established inhibitor of GLI-mediated gene transactivation.[29] GANT61 treatment successfully reduced GLI binding to the target sequence (Fig. 6c). In that condition, MT-2 and TL-Om1 cells showed remarkable reduction of cell viability by GANT61 treatment in dose- and time-dependent manners (Fig. 6d,e), which may be caused by apoptosis (Fig. 6f).

Finally, we evaluated the pharmacological activity of GANT61 on primary ATL samples. Although GANT61 did not show a clear effect on PBMC derived from healthy donors and HTLV-1 carriers, its treatment specifically reduced the viability of ATL samples significantly (Fig. 7a). Flow cytometry demonstrated that GANT61 specifically killed CD4+ leukemic cells from ATL patients via apoptosis induction (Fig. 7b).

Discussion

A large number of efforts have collectively concluded that aberrant gene expression patterns contribute to the malignant characteristics in ATL and other neoplastic cells. In the present study, based on the careful analyses of patient samples, we have demonstrated that *EVC* is drastically overexpressed in mRNA and its protein can be specifically detected in ATL cells in contrast to normal CD4+ T-cells. To the best of our knowledge, this is the first report regarding EVC expression and function in lymphocytes. The results of the microarray indicate that *EVC* expression appears to be induced in accordance with disease progression. EVC1 protein expression is observed in dysplastic ATL cells derived from patients and a xenotransplantation model. Because the EVC family may be membrane-associated proteins (Fig. 4),[30] the present study provides us with the possibility that EVC expressions might be useful cell markers of HTLV-1-infected T-cells for future clinical purposes.

The EVC family has been identified initially as the responsible genes for one morphogenic disorder, Ellis van Creveld syndrome; it is also believed to play a role in the determination of body-axis or morphogenesis by usually bearing one step of the HH signaling pathway.[12,17–19] Knockout studies have demonstrated that EVC1 and EVC2 cooperatively act as positive modulators of the HH pathway in mouse fibroblasts and chondrocytes. However, abnormal EVC upregulation has not been reported in any cancers; whether the HH pathway is sensitive to cellular dynamism of EVC has not been elucidated as yet. Herein, we demonstrated that overexpression of EVC can be linked to HH activity in T cells for the first time. In addition, several experimental results, including the knockdown assay and GANT61 treatment, suggest totally that the HH pathway was activated in ATL, which in turn contributed to ATL cell survival. Further study will be required for mechanistic insights on how EVC activates HH in T cells.

Further investigation uncovered that transcription from the *EVC* locus was coordinated by epigenetic alteration. In particular, the lymphoma-associated H3Ac and H3K4me3 accumulations appeared to dominate EVC upregulation. Direct evidence from patient samples supported the epigenetic reprogramming, including previously unappreciated H3K4me3 rearrangements, conferring robust EVC expression. Interestingly, repressive histone mark H3K27me3 was mutually reduced at the *EVC* locus in the ATL samples, suggesting that cooperative regulation in this bivalent domain may define the EVC expression and possibly HH activity.

HTLV-1 Tax was involved in the regulation of EVC via epigenetic regulation. Nuclear localization-deficient Tax mutant was unable to induce EVC expression, implying that Tax may participate directly in determination of chromatin architecture. Indeed, lentiviral expression of Tax partially increased active histone modifications, which in turn activated HH signaling. Previously, we and others have reported that Tax physically binds with histone modifying factors, including HDAC,[31] SUV39H1[32] and SMYD3.[20] Interplay between Tax and epigenetic rearrangement may be closely involved in the progression of HTLV-1-infected cells to leukemic cells. Meanwhile, other ATL-specific epigenetic events including significant modifications on histone acetylation, H3K4me3 and H3K27me3 clearly dominate stable EVC expression. The alteration of the epigenetic landscape by Tax and other molecular mechanisms such as expression changes of epigenetic modifiers will be elucidated by comprehensive analysis such as a genome-wide ChIP analysis.

In the context of molecular targeting, a new possibility for the HH inhibitor was suggested. Recently, aberrant HH activation and its contribution to cell survival and the cell cycle have been reported in various cancer cells.[11,12] In agreement with other tumors where HH is active, we found that ATL was sensitive against GANT61. This compound can inhibit HH signaling by preventing DNA binding of the GLI family and has few impacts on the viability of healthy CD4+ T cells. We note that we could not confirm the EVC-directed upregulation of common HH target genes such as *Cyclin D1* and *Bcl-2* in ATL models (data not shown). Given that the HH pathway regulates transcription of many genes important for cell fate and many inhibitors against HH cascade have been developed,[16] our findings suggest that pharmacological drugs that can inhibit the HH pathway may be feasible for ATL treatment. Identification of ATL-specific HH target genes will help understanding of the HH roles in survival capability.

In summary, we have identified EVC overexpression as a specific character of ATL and HTLV-1-infected T cells. We have demonstrated the molecular mechanism that overexpressed EVC1 contributes to ATL cell survival. Considering aberrant gene expression associated with cancers, the emerging relationship between epigenetic regulation and the HH pathway provides us with conceptual advance in understanding the broad-acting oncogenic signaling.

Acknowledgments

The authors thank Dr M. Iwanaga and Ms T. Akashi for support and maintenance of JSPFAD and Mr Y. Sasaki for experimental support of the IHC study. The authors also thank Drs H. Miyoshi and A. Miyawaki for providing the Venus-encoding lentivirus vectors and Dr S. Okada for providing the NOJ mice. This work is supported by JSPS KAKENHI Grant Numbers 24790436 (M.Y.) and 23390250 (T.W.), MEXT KAKENHI Grant Number 221S0001 (T.W.), Grant-in-Aid from the Ministry of Health, Labour and Welfare H24-Third Term Cancer-004 (T.W.), and a grant from the Uehara Memorial Foundation (M.Y.).

Disclosure Statement

The authors have no conflict of interest.

References

1 Uchiyama T, Yodoi J, Sagawa K, Takatsuki K, Uchino H. Adult T-cell leukemia: clinical and hematologic features of 16 cases. *Blood* 1977; **50**: 481–92.
2 Poiesz BJ, Ruscetti FW, Gazdar AF, Bunn PA, Minna JD, Gallo RC. Detection and isolation of type C retrovirus particles from fresh and cultured lymphocytes of a patient with cutaneous T-cell lymphoma. *Proc Natl Acad Sci USA* 1980; **77**: 7415–9.
3 Yoshida M, Miyoshi I, Hinuma Y. Isolation and characterization of retrovirus from cell lines of human adult T cell leukemia and its implication in the disease. *Proc Natl Acad Sci USA* 1982; **79**: 2031–5.
4 Tsukasaki K, Utsunomiya A, Fukuda H *et al.* VCAP-AMP-VECP compared with biweekly CHOP for adult T-cell leukemia–lymphoma: Japan Clinical Oncology Group Study JCOG9801. *J Clin Oncol* 2007; **25**: 5458–64.
5 Yamagishi M, Nakano K, Miyake A *et al.* Polycomb-mediated loss of miR-31 activates NIK-dependent NF-κB pathway in adult T cell leukemia and other cancers. *Cancer Cell* 2012; **21**: 121–35.
6 Yamagishi M, Watanabe T. Molecular hallmarks of adult T cell leukemia. *Front Microbiol* 2012; **3**: 334.
7 Grassmann R, Aboud M, Jeang KT. Molecular mechanisms of cellular transformation by HTLV-1 Tax. *Oncogene* 2005; **24**: 5976–85.
8 Hall WW, Fujii M. Deregulation of cell-signaling pathways in HTLV-1 infection. *Oncogene* 2005; **24**: 5965–75.
9 Mori N, Fujii M, Ikeda S *et al.* Constitutive activation of NF-kappaB in primary adult T-cell leukemia cells. *Blood* 1999; **93**: 2360–8.
10 Watanabe M, Ohsugi T, Shoda M *et al.* Dual targeting of transformed and untransformed HTLV-1-infected T cells by DHMEQ, a potent and selective inhibitor of NF-kappaB, as a strategy for chemoprevention and therapy of adult T-cell leukemia. *Blood* 2005; **106**: 2462–71.
11 Low JA, de Sauvage FJ. Clinical experience with Hedgehog pathway inhibitors. *J Clin Oncol* 2010; **28**: 5321–6.
12 Briscoe J, Thérond PP. The mechanisms of Hedgehog signalling and its roles in development and disease. *Nat Rev Mol Cell Biol* 2013; **14**: 416–29.
13 Johnson RL, Rothman AL, Xie J *et al.* Human homolog of patched, a candidate gene for the basal cell nevus syndrome. *Science* 1996; **272**: 1668–71.
14 Dierks C, Grbic J, Zirlik K *et al.* Essential role of stromally induced hedgehog signaling in B-cell malignancies. *Nat Med* 2007; **13**: 944–51.
15 Singh RR, Kim JE, Davuluri Y *et al.* Hedgehog signaling pathway is activated in diffuse large B-cell lymphoma and contributes to tumor cell survival and proliferation. *Leukemia* 2010; **24**: 1025–36.
16 McMillan R, Matsui W. Molecular pathways: the hedgehog signaling pathway in cancer. *Clin Cancer Res* 2012; **18**: 4883–8.
17 Tompson SWJ, Ruiz-Perez VL, Blair HJ *et al.* Sequencing EVC and EVC2 identifies mutations in two-thirds of Ellis-van Creveld syndrome patients. *Hum Genet* 2007; **120**: 663–70.
18 Ruiz-Perez VL, Blair HJ, Rodriguez-Andres ME *et al.* Evc is a positive mediator of Ihh-regulated bone growth that localises at the base of chondrocyte cilia. *Development* 2007; **134**: 2903–12.
19 Dorn KV, Hughes CE, Rohatgi R. A Smoothened-Evc2 complex transduces the Hedgehog signal at primary cilia. *Dev Cell* 2012; **23**: 823–35.
20 Yamamoto K, Ishida T, Nakano K *et al.* SMYD3 interacts with HTLV-1 Tax and regulates subcellular localization of Tax. *Cancer Sci* 2011; **102**: 260–6.
21 Sasaki H, Hui C, Nakafuku M, Kondoh H. A binding site for Gli proteins is essential for HNF-3beta floor plate enhancer activity in transgenics and can respond to Shh *in vitro*. *Development* 1997; **124**: 1313–22.
22 Yamagishi M, Ishida T, Miyake A *et al.* Retroviral delivery of promoter-targeted shRNA induces long-term silencing of HIV-1 transcription. *Microbes Infect* 2009; **11**: 500–8.
23 Miyoshi H, Takahashi M, Gage FH, Verma IM. Stable and efficient gene transfer into the retina using an HIV-based lentiviral vector. *Proc Natl Acad Sci USA* 1997; **94**: 10319–23.

24 Miyoshi H, Blömer U, Takahashi M, Gage FH, Verma IM. Development of a self-inactivating lentivirus vector. *J Virol* 1998; **72**: 8150–7.
25 Kobayashi S, Nakano K, Watanabe E *et al.* CADM1 expression and stepwise downregulation of CD7 are closely associated with clonal expansion of HTLV-I-infected cells in adult T-cell leukemia/lymphoma. *Clin Cancer Res* 2014; **20**: 2851–61.
26 Sasaki D, Imaizumi Y, Hasegawa H *et al.* Overexpression of enhancer of zeste homolog 2 with trimethylation of lysine 27 on histone H3 in adult T-cell leukemia/lymphoma as a target for epigenetic therapy. *Haematologica* 2011; **96**: 712–9.
27 Smith MR, Greene WC. Identification of HTLV-I tax trans-activator mutants exhibiting novel transcriptional phenotypes. *Genes Dev* 1990; **4**: 1875–85.
28 Tsuji T, Sheehy N, Gautier VW, Hayakawa H, Sawa H, Hall WW. The nuclear import of the human T lymphotropic virus type I (HTLV-1) tax protein is carrier- and energy-independent. *J Biol Chem* 2007; **282**: 13875–83.
29 Lauth M, Bergström A, Shimokawa T, Toftgård R. Inhibition of GLI-mediated transcription and tumor cell growth by small-molecule antagonists. *Proc Natl Acad Sci USA* 2007; **104**: 8455–60.
30 Blair HJ, Tompson S, Liu YN *et al.* Evc2 is a positive modulator of Hedgehog signalling that interacts with Evc at the cilia membrane and is also found in the nucleus. *BMC Biol* 2011; **9**: 14.
31 Ego T, Ariumi Y, Shimotohno K. The interaction of HTLV-1 Tax with HDAC1 negatively regulates the viral gene expression. *Oncogene* 2002; **21**: 7241–6.
32 Kamoi K, Yamamoto K, Misawa A *et al.* SUV39H1 interacts with HTLV-1 Tax and abrogates Tax transactivation of HTLV-1 LTR. *Retrovirology* 2006; **3**: 5.

Supporting Information

Additional supporting information may be found in the online version of this article:

Fig. S1. HTLV-1 *HBZ* does not affect EVC expression.

Fig. S2. EVC knockdown reduces ATL cell proliferation.

Methods S1. Including: details of clinical samples; and primer sequences used in the present study.

OPEN ACCESS Freely available online

PLOS ONE

Trans-Homophilic Interaction of CADM1 Activates PI3K by Forming a Complex with MAGuK-Family Proteins MPP3 and Dlg

Shigefumi Murakami[◔], **Mika Sakurai-Yageta**[◔], **Tomoko Maruyama, Yoshinori Murakami***

Division of Molecular Pathology, Institute of Medical Science, The University of Tokyo, Tokyo, Japan

Abstract

CADM1 (Cell adhesion molecule 1), a cell adhesion molecule belonging to the immunoglobulin superfamily, is involved in cell-cell interaction and the formation and maintenance of epithelial structure. Expression of CADM1 is frequently down-regulated in various tumors derived from epithelial cells. However, the intracellular signaling pathways activated by CADM1-mediated cell adhesion remain unknown. Here, we established a cell-based spreading assay to analyze the signaling pathway specifically activated by the *trans*-homophilic interaction of CADM1. In the assay, MDCK cells expressing exogenous CADM1 were incubated on the glass coated with a recombinant extracellular fragment of CADM1, and the degree of cell spreading was quantified by measuring their surface area. Assay screening of 104 chemical inhibitors with known functions revealed that LY294002, an inhibitor of phosphoinositide 3-kinase (PI3K), efficiently suppressed cell spreading in a dose-dependent manner. Inhibitors of Akt and Rac1, downstream effectors of PI3K, also partially suppressed cell spreading, while the addition of both inhibitors blocked cell spreading to the same extent as did LY294002. Furthermore, MPP3 and Dlg, membrane-associated guanylate kinase homologs (MAGuK) proteins, connect CADM1 with p85 of PI3K by forming a multi-protein complex at the periphery of cells. These results suggest that *trans*-homophilic interaction mediated by CADM1 activates the PI3K pathway to reorganize the actin cytoskeleton and form epithelial cell structure.

Citation: Murakami S, Sakurai-Yageta M, Maruyama T, Murakami Y (2014) *Trans*-Homophilic Interaction of CADM1 Activates PI3K by Forming a Complex with MAGuK-Family Proteins MPP3 and Dlg. PLoS ONE 9(2): e82894. doi:10.1371/journal.pone.0082894

Editor: *Antimo Migliaccio, Il Università di Napoli, Italy*

Received April 26, 2013; **Accepted** November 7, 2013; **Published** February 4, 2014

Funding: This work was supported by a Grant-in-Aid for Scientific Research (B) [22300336 and 25290051 for Y.M.]; a Grant-in-Aid for Young Scientists (B) [21790309 and 24790310 for M.SY.]; from the Ministry of Education, Culture, Sports, Science, and Technology, Japan; and a Grant-in-Aid for the Third Term Comprehensive Control Research for Cancer from the Ministry of Health, Labor, and Welfare, Japan [22090601 and 23120701 for Y.M.]. The authors also thank the Screening Committee of Anticancer Drugs, supported by a Grant-in-Aid for Scientific Research in the Priority Area "Cancer" from The Ministry of Education, Culture, Sports, Science, and Technology, Japan, for the SCADS inhibitor kit. The funders had no role in study design, data collection and analysis, decision to publish, or preparation of the manuscript.

Competing Interests: The authors declare that no competing interests exist.

* Email: ymurakam@ims.u-tokyo.ac.jp

◔ These authors contributed equally to this work.

Introduction

Cell surface proteins are important for recognizing the external environment and transmitting the information to the cytoplasmic regions through intracellular signaling pathways. Cell responses, such as proliferation, differentiation, apoptosis, or migration, are determined by different signaling pathways. Recently, cell adhesion molecules (CAMs)' role in signal transduction has emerged in addition to their classical roles in cell adhesions [1,2]. CAMs interact with growth factor receptors on plasma membranes or adaptor molecules in juxtamembrane regions. For instance, N-cadherin and NCAM interact with FGFR to promote its signaling in neuronal cells [3]. In epithelial cells, E-cadherin recruits β-catenin in its cytoplasmic domain to organize cell adhesion machinery. However, once intracellular adhesion by E-cadherin is abrogated, E-cadherin and β-catenin dissociate from each other, and β-catenin acts as an important effector in the Wnt signaling pathway; free β-catenin accumulates in the cytoplasm, moves into the nucleus, and then stimulates the transactivation of TCF/LEF for cell proliferation [4].

Cell adhesion molecule 1 (CADM1), cell adhesion molecules of the immunoglobulin superfamily (IgCAMs), contains three extracellular Ig-like loops, a single transmembrane domain, and a short intracellular carboxy-terminal tail [5]. CADM1 is also known as TSLC1, Necl-2, IgSF4A, and SynCAM1 [6]. CADM1 is expressed diffusely in the lateral membrane of cell-cell attachment sites in polarized epithelia, whereas, expression of CADM1 is frequently lost or reduced in a variety of advanced-stage human cancers of the lung, prostate, liver, pancreas, and breast [6]. Considering that the disruption of cell-cell adhesion in epithelial cells triggers tumor cell invasion and metastasis, CADM1 is one of the crucial tumor suppressors involved in cell adhesion like E-cadherin. In fact, CADM1 has a cell aggregation activity when introduced into MDCK cells lacking endogenous CADM1 expression. However, the cytoplasmic signaling pathways triggered by *trans*-homophilic interaction of CADM1 have not been fully elucidated.

The cytoplasmic domain of CADM1 in 46 amino acids contains a protein 4.1-binding motif and a class II PSD95/Dlg/ZO-1 (PDZ)-binding motif. We have demonstrated that CADM1 is

connected to the actin cytoskeleton through direct interaction with protein 4.1B [7]. CADM1 also associates with members of a group of scaffolding proteins, membrane-associated guanylate kinase homologs (MAGuKs), including MPP1-3, CASK, and Pals-2, through a class II PDZ-binding motif [8–11]. MAGuKs contain multiple protein-protein interaction modules, including PDZ, SH3, and GuK domains, that allow the clustering of transmembrane proteins and MAGuKs themselves [12]. In neuronal synapses, many MAGuKs, such as PSD-95, SAP102, SAP97/hDlg, and CASK, are localized at pre- and post-synaptic regions and are implicated in synaptic plasticity through the clustering of receptors [13]. In addition, one MAGuK, CARMA1, associates with PKC-θ and Bcl10 and activates NFκ-B signaling in T cells [14]. Thus, MAGuK-family proteins appeared to be important downstream molecules of CAMs, including CADM1, for intracellular signal transduction. However, the precise role of the interaction of CADM1 with MAGuKs remains to be understood.

In the present study, we established a cell-based assay to identify signaling pathways involved in cell spreading mediated by *trans*-homophilic interaction of CADM1. Distinct from a simple cell adhesion, cell spreading is a process that requires cytoplasmic signaling to generate actin reorganization mediated by *trans*-homophilic interaction of CADM1. By treating cells with 104 different chemical inhibitors with known target pathways, we identified that phosphoinositide 3-kinase (PI3K) signaling leading to actin rearrangement was essential for CADM1-mediated cell spreading. We further demonstrated that CADM1 was connected to PI3K by forming a protein complex with MPP3 and Dlg at the cell-cell contact sites.

We propose that CADM1 is implicated in transmitting cell attachment signals to actin reorganization in the cytoplasm through activating the PI3K pathway for the formation and maintenance of adhesion-based epithelial structure.

Materials and Methods

Expression Vectors, Cell Culture, Transfection, Antibodies, Reagents, Immunoprecipitation, Western Blotting, and Cell Aggregation Assay

These are described in detail in the Methods S1.

Purification of Recombinant CADM1-EC-Fc

HEK293 cells stably expressing a secreted form of CADM1-EC-Fc were cultured in GIT medium for 3 days after the cells reached confluence (Wako Pure Chemical Industries, Ltd., Osaka, Japan). Then, the conditioned medium was collected, and CADM1-EC-Fc was purified using the Affi-Gel Protein A MAPS II kit (Bio-Rad) and dialyzed against phosphate-buffered saline (PBS).

Cell Spreading Assay

Coverslips were pre-coated with 50 μg/ml of poly-L-lysine (Sigma-Aldrich) and fixed with 0.5% glutaraldehyde (Sigma-Aldrich) in 24-well plates. The glasses were then incubated with 50 nM of CADM1-EC-Fc or control mouse IgG for 10 min and blocked with 1% bovine serum albumin (BSA, Sigma-Aldrich) in Hank's Balanced Salt Solution (HBSS) (Invitrogen). Then, MDCK cells (3×10^4) were plated on the glasses and incubated at 37°C for 60–70 min as indicated. After incubation, cells were fixed with 4% paraformaldehyde and subjected to immunofluorescence labeling with Alexa Fluor-labeled phalloidin. Cells were imaged with an epifluorescence microscope (Zeiss), and the surface area of GFP positive cells was measured by the AutoMeasure software module, AxioVision Version 4 (Zeiss). To evaluate the activities of inhibitors, the surface area of cells with each inhibitor was normalized to that of cells on IgG with DMSO, and then the value of cells on CADM1-EC-Fc with DMSO was set as 1. More than 100 cells were counted, at least, for each assay as indicated in the legend for each Figure as reported previously [15]. Statistical differences were determined by Student's t-test.

Immunofluorescence Microscopy

Cells were fixed with 4% paraformaldehyde for 20 min, quenched with 50 mM of NH_4Cl, and permeabilized with 0.1% Triton X-100 in PBS for 5 min. Cells were then blocked with 5% (w/v) fetal bovine serum in phosphate-buffered saline (PBS) and then incubated with primary and secondary antibodies sequentially with extensive washes between the incubation of different antibodies. Coverslips were then mounted with ProLong® Gold (Invitrogen), and cells were imaged with the epifluorescence microscope (Zeiss). Negative controls without primary antibodies were included in all experiments.

Glutathione S-transferase (GST) Pull-down Assay

The GST- or His-fusion protein was expressed in Rosetta DE3 *Escherichia coli* and isolated with glutathione Sepharose 4B (GE Healthcare) or Ni-NTA Agarose (QIAGEN), respectively, according to the manufacturers' protocols. For *in vitro* binding, the His-MPP3-N protein was incubated with GST-fusion proteins of CADM1 for 15 min at 4°C in a reaction buffer (50 mM of Tris-HCl, pH 7.4, 137 mM of NaCl, 0.1% Triton X-100, 10% glycerol, 0.5% BSA). The His-Dlg-N protein was added and incubated for 15 min, and then Glutathione Sepharose beads were added and further incubated for 1 h at 4°C. Beads were washed with reaction buffer and subjected to SDS-PAGE and Western blotting with anti-His antibodies. GST fusion proteins were detected by staining with Coomassie Brilliant Blue (CBB).

Results

Recombinant Extracellular Domain of CADM1 Mimics *Trans*-Homophilic Interaction of CADM1 and Induces Cell Spreading

We first established this cell spreading assay to identify the signaling pathway specifically activated by *trans*-homophilic interaction of CADM1 mediated by intercellular adhesion. MDCK cells stably expressing CADM1-GFP (MDCK+CADM1-GFP) or parental MDCK cells were incubated on the glass coated either with mouse IgG or with the recombinant CADM1-EC-Fc protein consisting of the extracellular fragment domain of CADM1 fused to the Fc region of mouse IgG. The following immunofluorescence staining of the actin cytoskeleton revealed that MDCK+CADM1-GFP cells showed large spread morphology when incubated on CADM1-EC-Fc-coated glass. By contrast, parental MDCK cells incubated on IgG- or CADM1-EC-Fc-coated glass or MDCK+CADM1-GFP cells incubated on IgG-coated glass showed round but not spread morphology (Fig. 1A and S1A). When the surface of the cells was measured quantitatively, the average surface area of MDCK+CADM1-GFP cells on CADM1-EC-Fc was 1.8-fold larger than that of the same cells on control IgG, although the size of the surface area was varied in each cell (Fig. 1B). To confirm that the spreading of the cells observed is mediated by *trans*-homophilic interaction of CADM1, the same assay was performed in the presence of the anti-CADM1 antibody, 9D2, which was shown to act as a blocking antibody [16]. As shown in Fig. S1B and 1B, the surface area of MDCK+CADM1-GFP cells incubated on CADM1-EC-Fc decreased significantlywhen incubated with the 9D2 antibody,

whereas the area was not changed with control IgY. Moreover, the surface area of MDCK+CADM1-GFP cells was not changed by 9D2 when incubated on IgG. These results suggest that cell spreading in this assay was specifically induced by the *trans*-homophilic interaction of CADM1. Since the actin cytoskeleton is one of the main determinants of cell shape, we then investigated the effect of Cytochalasin D, an inhibitor of actin polymerization, on CADM1-mediated cell spreading. As shown in Fig. S1C and 1C, spreading of MDCK+CADM1-GFP cells on CADM1-EC-Fc-coated glass was abrogated by Cytochalasin D, but not by control DMSO. These findings suggest that the *trans*-homophilic interaction of CADM1 induces cell spreading through reorganization of the actin cytoskeleton.

Next, we investigated whether the cytoplasmic domain of CADM1 is responsible for cell spreading. To examine this, MDCK cells were stably transfected with an expression vector of a truncated form of CADM1 lacking its cytoplasmic domain that was fused to YFP (ΔCT-YFP) and subjected to cell spreading assay (Fig. 1D). It should be noted that CADM1-ΔCT-YFP was localized at cell-cell contact sites similarly to full-length CADM1 tagged with YFP (FL-YFP) in confluent MDCK cells (Fig. S1D). The surface area of MDCK cells expressing CADM1-ΔCT-YFP is significantly smaller than that of CADM1-FL-YFP cells and not different from that of MDCK cells with CADM1-ΔCT-YFP incubated on control IgG (Fig. S1E and 1E). These findings suggest that the cytoplasmic domain of CADM1, and its cytoplasmic binding proteins as well, is essential for activating signaling for the actin reorganization to lead to cell spreading.

The PI3K Inhibitor Suppresses the Cell Spreading Mediated by *Trans*-homophilic Interaction of CADM1

The above findings prompted us to investigate the signaling pathway activated by CADM1-mediated cell adhesion to induce actin reorganization using cell spreading assay by treating cells with chemical compounds from the SCADS inhibitor kit (see Materials and Methods) and assessing the suppressor activity of each inhibitor in cell spreading. Among 104 chemicals we screened, two inhibitors of PI3K, LY294002 and Wortmannin, effectively suppressed cell spreading (Fig. S2A). The average cell areas treated with LY294002 and Wortmannin are 53% and 54%, respectively, in comparison with that treated with DMSO as 100%. On the other hand, the average cell surface areas treated with inhibitors of MAPK, JAK, and NF-KB in the same assay were 94%, 109%, and 96%, respectively, suggesting that the suppressor effect in cell spreading by PI3K inhibitors is significant. To confirm this inhibitory effect precisely, cells were then treated with different concentrations of LY294002, from 0.01 to 10 μM, and subjected to cell spreading assay. As shown in Fig. S2B and 2A, the surface area decreased by the treatment of LY294002 in a dose-dependent manner, where a significant difference was observed when it was treated with 1 and 10 μM of LY294002 as compared with DMSO. To exclude the possibility that LY294002 has a non-specific cytotoxic effect, cells were treated with 1 μM of LY294002 for 45 min and then washed and incubated with a fresh medium without LY294002 for an additional 45 min. Comparison of the surface area of cells revealed that cell spreading was suppressed in the presence of LY294002 for 90 min, while the suppressing effect was abrogated and the cell spreading was recovered when LY294002 was washed out (Fig. S2C and 2B), indicating that cell spreading was not irreversibly suppressed by the cytotoxicity of LY294002. Since the *trans*-homophilic interaction of CADM1 has been shown to induce cell aggregation in a suspension culture, we next examined the activity of LY294002 on CADM1-mediated cell aggregation. When cell aggregation assay was carried out, the degree of aggregate formation in cells treated with various concentrations of LY294002 did not show significant difference from that of DMSO-treated cells (Fig. 2C), showing that PI3K is not involved in intercellular adhesion activity by CADM1. These results suggest that CADM1-mediated *trans*-homophilic interaction activates PI3K to induce cell spreading but does not participate in cell aggregation activity.

Activation of the Pathways Downstream of PI3K, Akt, and Rac1 Is Necessary for CADM1-mediated Cell Spreading

Then, we analyzed how PI3K was activated by CADM1-mediated cell attachment to lead cell spreading. Since PIP_3 is a major product of PI3K signaling at the plasma membrane and specifically binds to the PH domain of Akt [17], PI3K activity can be detected by the exogenously expressed fluorescent Akt-PH in the cells. Here, to examine PI3K activation and its subcellular localization, MDCK cells expressing CADM1 without tags (MDCK+CADM1) were transiently transfected with a protein fragment of the PH domain of Akt tagged with GFP (GFP-Akt-PH) and subjected to spreading assay. After 45 min of incubation on a CADM1-EC-Fc-coated plate, strong signals of GFP-Akt-PH were detected at the leading edges of MDCK+CADM1 cells where actin-rich lamellipodia were generated, indicating that PI3K is activated at the leading edges of cells in CADM1-induced cell spreading (Fig. 3A).

We further examined the activation of Akt, a well-established downstream target of PI3K for actin remodeling, in CADM1-mediated cell spreading [18]. In Western blotting analysis, the increased intensity of the signal from phosphorylated Akt was detected in MDCK+CADM1-GFP cells cultured on the CADM1-EC-Fc-coated plate as compared with that of the cells on IgG, whereas no signal was detected when cells were treated with 10 μM of LY294002 (Fig. 3B). These results suggest that phosphorylation of Akt participates in CADM1-mediated cell spreading as a possible downstream effector of the PI3K pathway. However, when examined in the cell spreading assay, the inhibitor of Akt only partially suppressed spreading of MDCK+CADM1-GFP cells as compared with LY294002 when cultured on CADM1-EC-Fc, suggesting that some additional effectors would participate in the PI3K signaling (Fig. 3C). Then we examined Rac1, another effector of PI3K implicated in actin remodeling [19]. As shown in Fig. S2D and 3C, the Rac1 inhibitor only partially suppressed CADM1-mediated cell spreading as compared with LY294002 as the Akt-inhibitor did. However, when cells were treated with both Akt- and Rac1- inhibitors simultaneously, the surface area of MDCK+CADM1 cells decreased dramatically without any significant difference from those treated with LY294002, indicating that the Akt- and Rac1- inhibitors worked additively to suppress cell spreading. These findings indicate that both Akt and Rac1 are key effectors of PI3K when activated by CADM1-mediated cell spreading.

CADM1 Forms a Multi-protein Complex with MPP3, Dlg, and PI3K

Finally, we analyzed possible molecules that connect CADM1 with PI3K leading to cell spreading. It has been reported that the regulatory subunit of PI3K, p85, interacts with one MAGuK, Dlg, and is recruited to cell-cell contact sites in epithelial cells [20]. Dlg further binds to another MAGuK, MPP3, which was identified as a binding partner of the cytoplasmic domain of CADM1 through their N-terminal domain [8,21], suggesting that MPP3 and Dlg are candidates for connecting CADM1 with PI3K. To examine

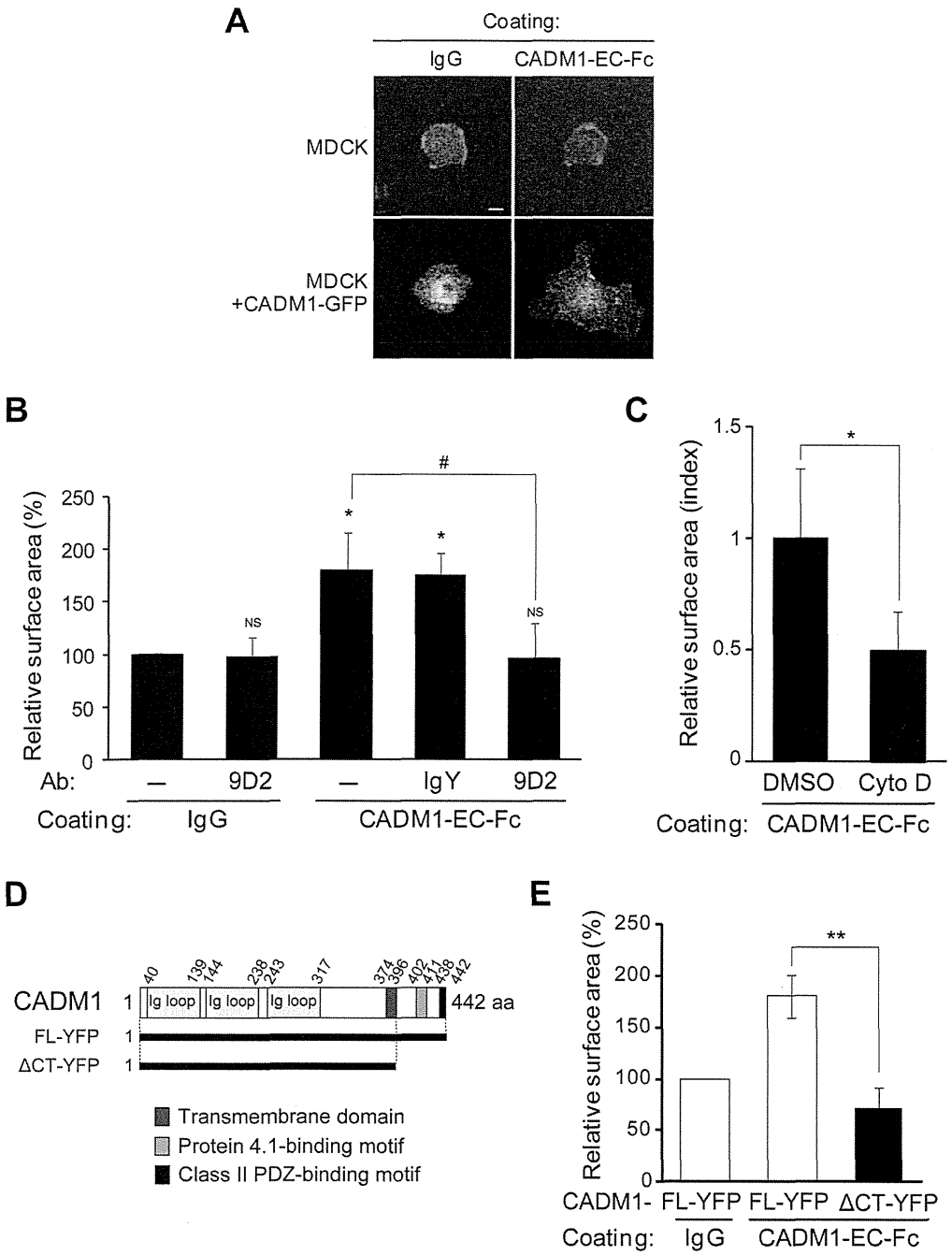

Figure 1. Recombinant extracellular domain of CADM1 mimics the *trans*-homophilic interaction of CADM1 and induces cell spreading. Parental MDCK cells or MDCK cells stably expressing CADM1-GFP (MDCK+CADM1-GFP) were incubated on coverslips coated with control IgG or recombinant proteins consisting of the extracellular fragment of CADM1 fused to Fc fragments of mouse IgG (CADM1-EC-Fc). After 60 min, the cells were visualized by staining the actin cytoskeleton with Alexa Fluor 568-labeled phalloidin. (A) Representative images of F-actin in cells incubated on control IgG- or CADM1-EC-Fc-coated glasses as indicated. Bars: 20 μm. (B) MDCK+CADM1-GFP cells were incubated on IgG or CADM1-EC-Fc in the presence or absence of control human IgG or anti-CADM1 antibody, 9D2 (10 μg/ml). Cell spreading was quantified by measuring the average surface area of cells. Relative value to cells on the IgG-coated glass without antibodies was shown. More than 100 cells were counted in the assay. *, $p<0.05$; NS, no significant difference (vs. cells on IgG without antibodies). #, $p<0.05$. (C) Cell spreading assay using MDCK+CADM1-GFP cells incubated on IgG or CADM1-EC-Fc with DMSO or 1 μM of Cytochalasin D (Cyto D). The area was normalized to that of cells on IgG with DMSO, and the relative value to cells on CADM1-EC-Fc with DMSO was shown. More than 180 cells were counted in the assay. *, $p<0.05$. (D) A schematic representation of CADM1 protein structure. The YFP-fusion proteins of full-length CADM1 (CADM1-FL) and its deletion mutant lacking the cytoplasmic fragment (CADM1-ΔCT) were shown. (E) Cell spreading assay of MDCK cells stably expressing CADM1-YFP-FL or CADM1-YFP-ΔCT that were incubated on IgG or CADM1-EC-Fc. Relative value of cell surface area to that of CADM1-YFP-FL cells on IgG-coated glass was shown. More than 230 cells were counted in the assay. **; $p<0.01$. (B, C, and E) The results presented are mean ± SD of three independent experiments.
doi:10.1371/journal.pone.0082894.g001

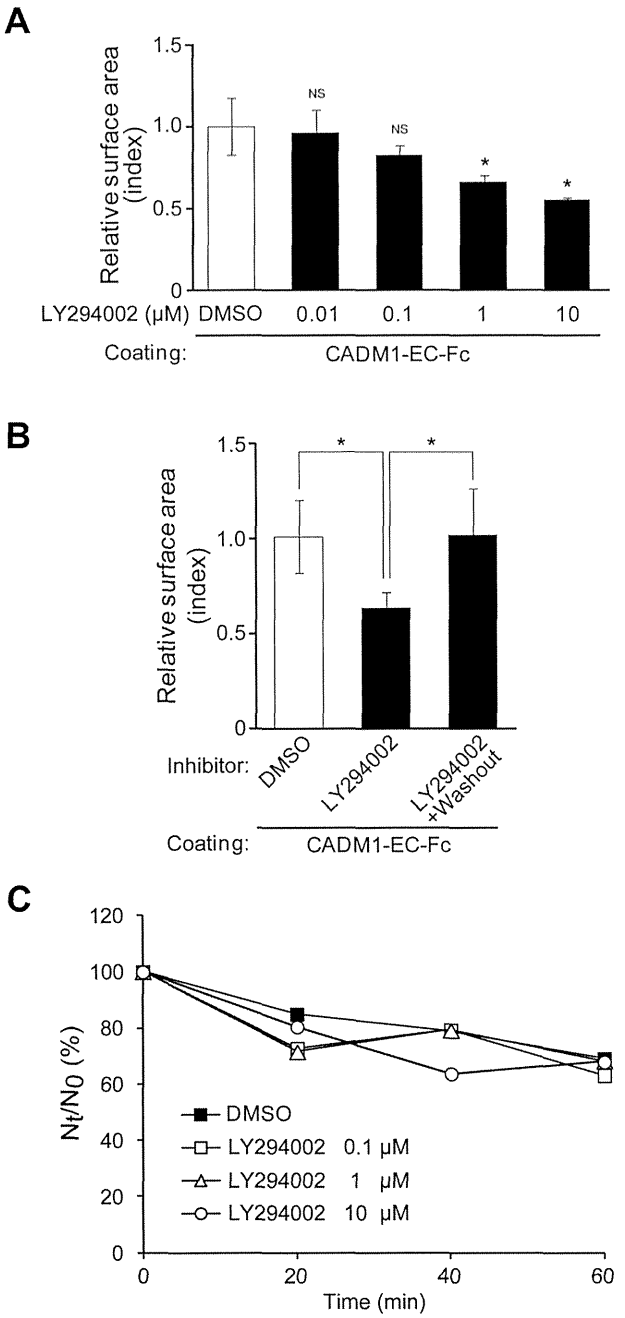

Figure 2. Two distinct inhibitors of PI3K suppress cell spreading mediated by *trans*-homophilic interaction of CADM1. (A) Cell spreading assay of MDCK+CADM1-GFP cells incubated on IgG or CADM1-EC-Fc in the presence of an inhibitor of PI3K, LY294002, from concentrations of 0.01 μM to 10 μM as indicated. *, $p<0.05$; NS, no significant difference (vs. cells on CADM1-EC-Fc with DMSO). (B) Cell spreading assay was performed using MDCK+CADM1-GFP cells cultured on CADM1-EC-Fc with 1 μM of LY294002 for 45 min and then washed and further incubated for 45 min in the presence of the same concentration of LY294002 (LY294002) or DMSO (LY294002+— washout). Representative images of CADM1-GFP are shown at the top of each bar graph. The area was normalized to that of cells on IgG with DMSO, and the relative value of the cell surface area to that of cells on CADM1-EC-Fc with DMSO was shown. *, $p<0.05$. (A and B) The results presented are mean ± SD of three independent experiments. More than 200 and 280 cells were counted in A and B, respectively. (C) Aggregation assay of MDCK+CADM1-GFP cells in Ca^{2+}- and Mg^{2+}-free condition in the presence of LY294002 at the concentrations indicated. The cell aggregation was represented by the ratio of the total particle number at time *t* of incubation (Nt) to the initial particle number (N0). The data shown here indicate the average Nt/N0 in triplicate experiments.

doi:10.1371/journal.pone.0082894.g002

the possible association of these molecules, MDCK+CADM1-GFP cells were used because MDCK cells expressed significant amounts of endogenous MPP3 and Dlg proteins. We examined whether CADM1 interacts with Dlg, a key molecule in connecting with PI3K *in vitro*. For this purpose, fused proteins of GST with the cytoplasmic fragment of CADM1 (GST-CADM1-C), a derivative of GST-CADM1-C lacking C-terminal 4 amino acids corresponding to PDZ-binding motif (GST-CADM1-CΔ4), as well as His-tagged N-terminal fragments of MPP3 (His-MPP3-N) and His-tagged N-terminal fragments of Dlg (His-Dlg-N), were constructed as shown in Fig. 4A. GST pull-down assay was then performed by incubating GST-CADM1-C or GST-CADM1-CΔ4 with His-MPP3-N and/or His-Dlg-N. Western blotting analysis revealed that His-Dlg-N was recovered with GST-CADM1-C depending on the presence of His-MPP3-N (Fig. 4B). On the other hand, neither His-Dlg-N nor His-MPP3 was bound to GST or GST-CADM1-CΔ4. These results indicate that MPP3 connects CADM1 with Dlg through direct binding of the N-terminal region of MPP3 with the class II PDZ-binding motif of CADM1 and with the N-terminal region of Dlg. Next, we examined possible *in vivo* complex formation of CADM1 with MPP3, Dlg, and p85. We first demonstrated that CADM1, MPP3, Dlg, and p85 were endogenously expressed in Caco-2 cells and co-localized one another at the cell-cell contact sites (Fig. 4C). When Caco-2 cells were transiently transfected with MPP3-HA and the lysates were immunoprecipitated with anti-CADM1 antibodies, signals corresponding to MPP3-HA and Dlg were detected by Western blotting using antibodies specific to HA and Dlg, respectively (Fig. 4D, left). MPP3-HA and p85 were also co-immunoprecipitated with Dlg in the same Caco-2 lysates that expressed MPP3-HA (Fig. 4D, right). Furthermore, when endogenous CADM1 expression in Caco-2 cells was depleted by transfection of shRNA of CADM1, localization of MPP3, Dlg, and p85 at plasma membrane was almost abrogated (Fig. S3). Moreover, the spreading of cells as well as the accumulations of a protein complex of GFP-Akt-PH, MPP3, Dlg, and p85 to the periphery of spreading cells were also impaired in MDCK cells expressing CADM1-ΔCT or MDCK cells expressing wild-type CADM1 together with siDlg (Fig. S4). These results suggest that CADM1 indirectly interacts with p85 by forming a multi-protein complex with MPP3 and Dlg and participates in cell spreading.

Discussion

CADM1 is expressed along the lateral membrane of epithelial cells and is involved in the attachment, formation, and maintenance of epithelial structure by forming a *trans*-homophilic interaction with CADM1 from adjacent epithelial cells. In the present study, to investigate signal transduction induced by CADM1-mediated intercellular adhesion, we established a cell-based assay to reconstitute an initial process of CADM1 interaction as cell spreading. The spreading of cells observed in the assay was specifically induced by *trans*-homophilic interaction of CADM1 because spreading was only observed when CADM1 was present both in the cell surface and on the glass and was abrogated by CADM1-blocking antibodies. By adding chemical inhibitors of known function in the assay and evaluating the degree of suppression in cell spreading through measuring the surface

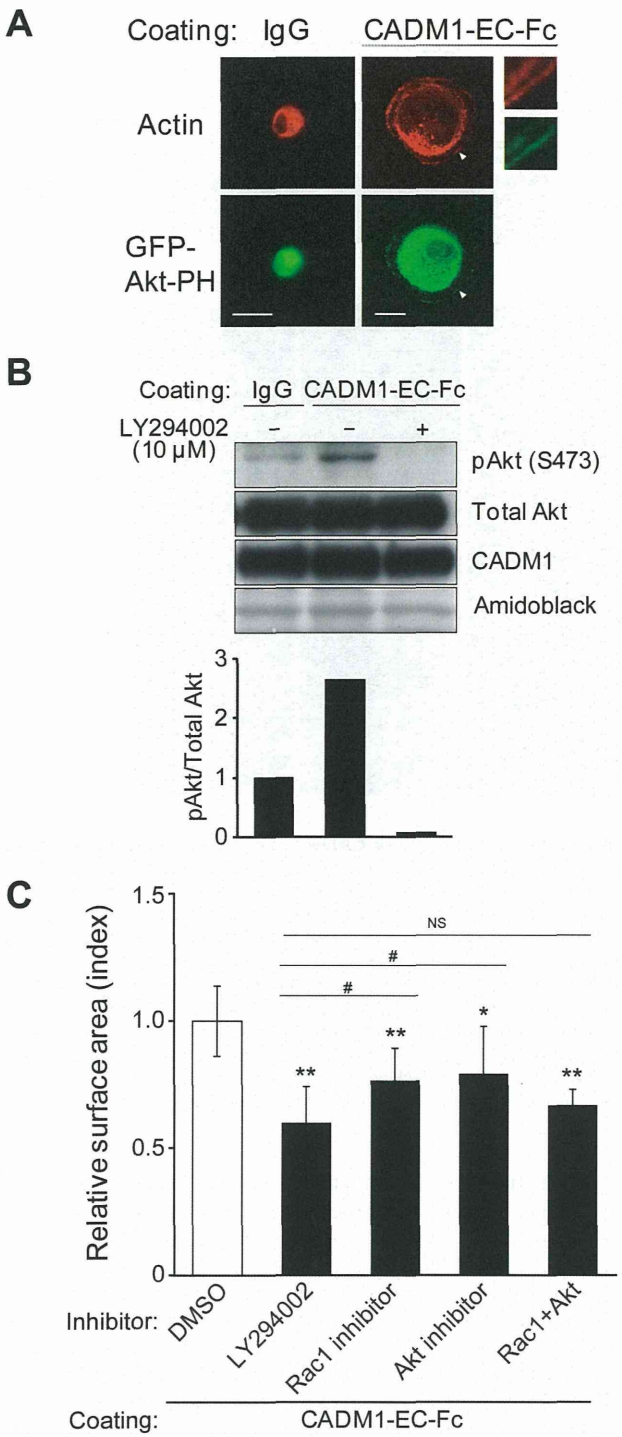

Figure 3. Activation of PI3K signaling is necessary for CADM1-mediated cell spreading. (A) MDCK cells stably expressing CADM1 were transiently transfected with GFP-Akt-PH and incubated on control IgG or CADM1-EC-Fc. Then, cells were visualized by staining with Alexa Fluor 568-labeled phalloidin. GFP-Akt-PH was observed at the periphery of the spreading cell where actin-rich lamellipodia were generated. High-magnification images of the region indicated by arrowhead were shown in the right panels. (B) Representative results of Western blotting analysis of phosphorylated-Akt, total Akt, and CADM1 using the lysates of MDCK+CADM1-GFP cells incubated on IgG or on CADM1-EC-Fc with DMSO (−) or with 10 μM of LY294002 (+). Note that the difference of signal intensities of Akt and p-Akt was due to the different sensitivities of antibodies and exposure time. The membrane was stained by Amido Black to confirm the equal loading of proteins. The amount of phosphorylated-Akt was normalized to that of the total Akt in each lane, and the relative value to cells on control IgG without LY294002 was calculated. The average scores of the relative values in 3 independent experiments are indicated in the lower panel. (C) MDCK+CADM1-GFP cells were incubated on control IgG or CADM1-EC-Fc in the presence of DMSO or 1 μM of the inhibitors of PI3K, Rac1 and/or Akt as indicated. The surface area was normalized to that of cells on IgG with DMSO, and the relative value to cells on CADM1-EC-Fc with DMSO was shown. The results presented are mean ± SD of five independent experiments. More than 470 cells were counted in the assay. *; $p<0.05$, **; $p<0.01$ (vs. cells on CADM1-EC-Fc with DMSO). #; $p<0.05$, NS; no significant difference (vs. cells on CADM1-EC-Fc with LY294002).
doi:10.1371/journal.pone.0082894.g003

area, signaling pathways activated by *trans*-homophilic interaction of CADM1 can be identified. Among 104 inhibitors screened in the assay, two independent inhibitors of PI3K, LY294002 and Wortmannin, suppressed the cell spreading most dramatically. The suppressor activity of LY294002 in cell spreading was reversible and dose-dependent. Furthermore, the cell spreading was reversibly inhibited by a PI3K inhibitor, LY294002, in a dose-dependent manner. Additionally, by visualizing the subcellular localization of PIP_3, a major product of PI3K, we demonstrated that PI3K was activated at the cell periphery where lamellipodia were generated. On the basis of these results, we speculate that CADM1 recruits PI3K to the cytoplasmic juxtamembrane domain to induce cell spreading. In addition to PI3K inhibitors, several known inhibitors showed partial activity in suppressing cell spreading. Some of them are related to PI3K signaling, like AKT or Rac1, while others appear to be independent of the PI3K pathways, which will be described elsewhere. MDCK cells were chosen in this assay because cell spreading was most dramatically and reproducibly observed in MDCK. In addition, we have previously demonstrated that MDCK cells transfected with a full length CADM1 showed suppressor effect in HGF-induced cell scattering in 2D-culture or tubulogenesis in 3D-culture but that transfection of CADM1ΔCT, CADM1 lacking 4.1-binding motif (CADM1Δ4.1BM), or CADM1 lacking PDZ-binding motif (CADM1ΔPDZBM) into MDCK lost the suppressor activity of scattering or tubulogenesis [27]. The functional significance of these molecules is then confirmed by transfecting shRNA of CADM1 or Dlg.

It has been demonstrated that CADM1 has potential to form heterophilic *trans*-interaction with other IgCAMs, such as CADM2/Necl-3, CADM3/Necl-1, Nectin-3, and CRTAM, depending on the types of cells [10,22]. Therefore, analyses of *trans*-heterophilic interactions of CADM1 with other molecules using similar cell-based assay would clarify different signaling pathways activated by specific types of cell adhesion.

Since the cytoplasmic domain of CADM1 was essential for cell spreading, we analyzed the intracellular pathways leading to activation of PI3K. On the basis of the following three pieces of evidence reported so far, we hypothesized that CADM1 would recruit PI3K through MAGuKs. (1) We, and others, showed that CADM1 associates with MAGuKs, such as MPP1-3, CASK, and Pals-2, through its class II PDZ-binding domain in epithelial cells [8–11]. (2) The SH2 domain of p85 interacts with Dlg, one of the MAGuKs carrying class I PDZ domain, when tyrosine residues of Dlg were phosphorylated [20]. (3) Several MAGuKs, such as MPP2, MPP3, CASK, and Dlg, bind to one another through their N-terminal L27 domain [21]. In the present study, we have demonstrated that CADM1 interacts with Dlg through MPP3 at

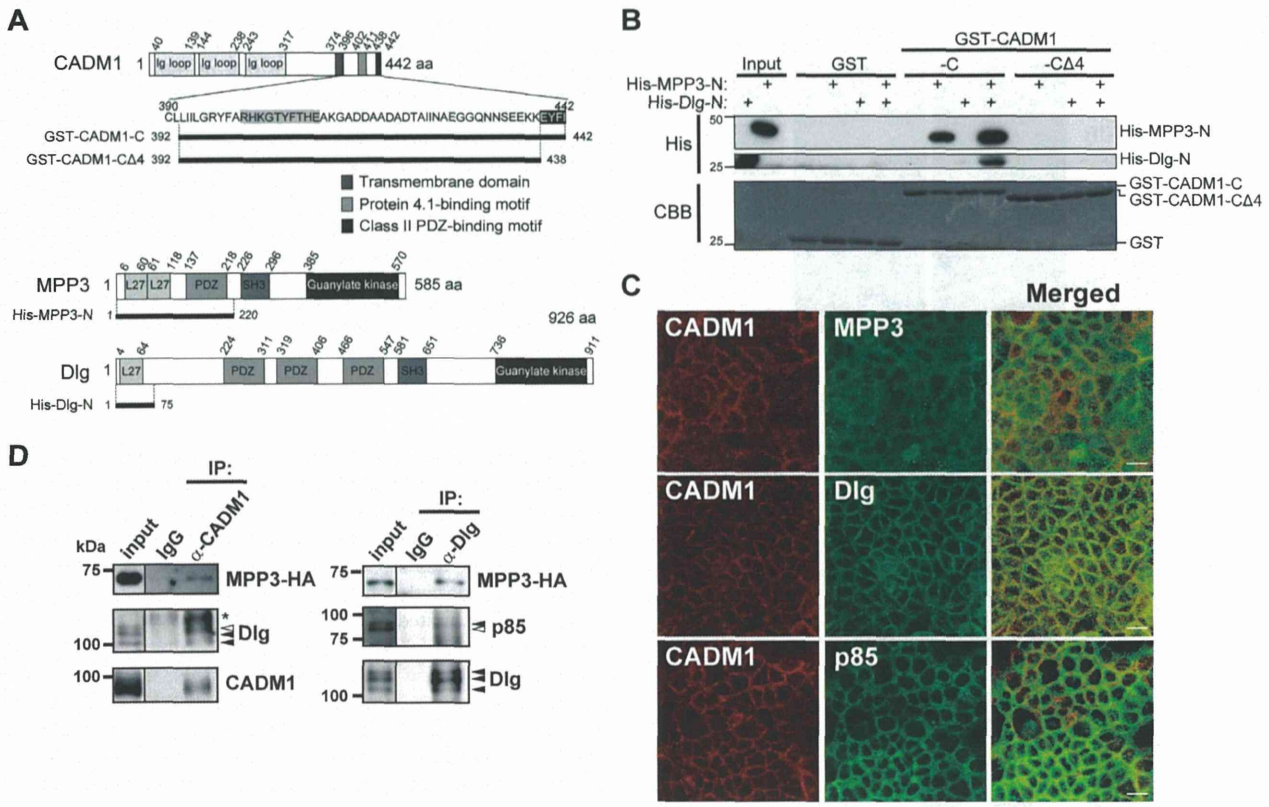

Figure 4. Membrane-associated guanylate kinase homologs (MAGuKs), MPP3 and Dlg, link CADM1 with p85 by forming a multi-protein complex. (A) *Schematic representation of the structures of CADM1, MPP3, and Dlg proteins. In amino acid sequences of the cytoplasmic* domain of CADM1, consensus sequences of 4.1- and class II PDZ-binding motifs are highlighted by grey and black, respectively. The GST-fusion protein of CADM1 with an entire cytoplasmic fragment (GST-CADM1-C) and a mutant form lacking a class II PDZ-binding motif (GST-CADM1- CΔ4) are *schematically represented below. N-terminal fragments of MPP3 and Dlg were purified as His-fusion proteins and used for an in vitro binding assay.* (B) Interaction of GST-CADM1 with His-MPP3 and/or His-Dlg was examined by GST pull-down assay. Binding proteins were detected by Western blotting using anti-His tag antibodies, whereas GST-fusion proteins were detected by staining the membrane with Coomassie Brilliant Blue (CBB). (C) *Localization of CADM1, MPP3, Dlg, and p85 in confluent Caco-2 cells. Confluent Caco-2 cells were fixed and stained with anti-CADM1 antibodies* (green) and anti-MPP3 (upper), anti-Dlg (middle), or anti-p85 (lower) antibodies (red). Merged images are shown in the right panel. Bars: 20 μm. (D) Lysates of Caco-2 cells expressing MPP3-HA were immunoprecipitated (IP) with control rabbit IgG and anti-CADM1 (left) or anti-Dlg (right) antibodies and analyzed by Western blotting with antibodies against HA, Dlg, p85, and CADM1, as indicated. Black arrowheads indicate signals found in both the input and immunoprecipitates, whereas white arrowheads indicate signals only found in the input. Asterisks show non-specific bands.
doi:10.1371/journal.pone.0082894.g004

the class II PDZ-binding motif *in vitro* using GST pull-down assay (Fig. 4B). Furthermore, we have shown that MPP3 and Dlg are co-immunoprecipitated with CADM1, while MPP3 and p85 are co-immunoprecipitated with Dlg by immunoprecipitation assay *in vivo* (Fig. 4D). By fluorescence microscopy analysis, we have also confirmed that CADM1 is co-localized with MPP3, Dlg, and p85 at the cell periphery (Fig. 4), whereas the recruitment of this protein complex to the cell periphery is abrogated by depletion of CADM1 or Dlg (Fig. S3 and Fig. S4). Taken together, these 4 proteins–CADM1, MPP3, Dlg, and p85–appear to form a complex at the juxtamembrane portion at the cell periphery and play an important role in cell spreading.

Cell spreading assay also identified Akt and Rac1 as possible molecules downstream of PI3K signaling when activated by the *trans*-homophilic interaction of CADM1. Both Akt and Rac1 are molecules known to be downstream of PI3K [19,23] in various cells, and we demonstrated that both Akt- and Rac1- inhibitors suppress spreading of MDCK cells significantly. However, quantitative measurement shows that the degree of suppression in cell spreading by Akt- or Rac1- inhibitors is only partial in comparison with that by PI3K inhibitor. On the other hand, when both an Akt- and Rac1- inhibitors are added simultaneously, cell spreading was fully suppressed. These findings demonstrate that Akt and Rac-1 act in the downstream of PI3K, but act independently of each other and that cell spreading assay has a great advantage in analyzing signaling pathways for its quantitative feature. These findings would be supported by our previous finding that Rac1 is sustained to be activated by HGF treatment when MDCK cells were transfected with full length CADM1 [26]. These findings might also be corresponding to another previous report by ours that introduction of dominant negative Rac1 suppressed lamellipodia formation of ATL cells when cultured on fibroblast, although ATL cells are not the epithelial origin [27]. Taken together, we propose a possible signaling pathway triggered by the *trans*-homophilic interaction of CADM1, as shown in Figure S5.

Expression of CADM1 is down-regulated in various carcinomas, and it is widely accepted that CADM1 is a tumor suppressor through its cell adhesive property. We have previously demonstrated that CADM1 is involved in the formation of epithelial cell structure since suppression of CADM1 expression by RNAi abrogated epithelial structure, induced simple flat morphology of

cells and inhibited the maturation of cell-cell adhesion [9]. PI3K has also emerged as a major regulator of the cytoskeleton and cell polarity [24]. It is quite interesting that inhibition of PI3K by LY294002 causes a reduction in cell height but does not affect cell adhesion activity in epithelial cells [25]. Our study also indicates that the inhibition of PI3K does not affect cell adhesion activity by *trans*-interaction of CADM1 but abrogates following cell spreading activity induced by cytoskeletal remodeling. Furthermore, it has been reported that Rac1 signaling is similarly implicated in the maintenance of cell height [25] and that PI3K-Rac1 signaling serves as a key regulator for inducing the extension of cell-cell contact zones [26]. Taken together, these findings suggest that *trans*-homophilic interaction of CADM1 acts as an initial trigger on the membrane for the formation and maintenance of epithelial cell structure by activating PI3K-Rac1 pathways to reorganize the actin cytoskeleton.

In this connection, it is noteworthy that we have previously reported that overexpression of CADM1 in MDCK cells suppresses hepatocyte growth factor (HGF)-induced epithelial-mesenchymal transition (EMT), which is a well-known phenomenon associated with cancer cell invasion and metastasis [27]. In CADM1 over-expressing cells, prolonged activation of Rac1 induced by CADM1 and its cytoplasmic binding proteins appeared to inhibit EMT induction by HGF through the retention of epithelial cell adhesion. Although we did not investigate the mechanism of Rac1 activation in the study, the MAGuK-PI3K pathway could be a candidate for activating Rac1 in cells over-expressing CADM1. Thus, CADM1 appears to act as a suppressor of cancer cell invasion and metastasis by its activity in the formation and maintenance of adhesion-based epithelial cell structure.

In this study, we have demonstrated that cell-based screening assay is an effective tool for identifying low-molecular-weight compounds that target signaling pathways mediated by *tarns*-homophilic interaction of CADM1. By screening known inhibitors that suppress cell spreading, we found that the PI3K pathway was specifically activated by *trans*-homophilic CADM1 interaction. The protein complex of CADM1-MPP3-Dlg appears to recruit PI3K to the juxtamembrane region to induce actin reorganization by activating Akt and Rac1. In conclusion, the PI3K pathway is crucial for the signals mediated by *trans*-homophilic CADM1 interaction to cytoplasm, leading to cytoskeletal remodeling and the formation and maintenance of epithelial structure.

Supporting Information

Figure S1 Establishment of cell spreading assay. (A) Representative images of cells analyzed by spreading assay shown in Fig. 1A. In each assay, 10 fields were imaged in duplicate and average area of cells were quantified by image J software. MDCK (a and b) and MDCK+CADM1-GFP (c and d) cells were put on IgG (a and c) or CADM1-EC-Fc (b and d), respectively, as indicated on top of images. Two fields of phalloidin-stained (a and b) and GFP (c and d) images are shown. Bars: 50 μm. (B, C, and E) Representative images of spreading assay shown in Fig. 1B (B), Fig. 1C (C), and Fig. 1E (E). Cells stained with phalloidin are shown. Bars: 50 μm. (D) Localization of CADM1-FL-YFP and -ΔCT-YFP in confluent MDCK cells. Confluent MDCK cells stably expressing CADM1-FL-YFP or -ΔCT-YFP were fixed and stained with phalloidin (red). Bars: 20 μm.
(TIF)

Figure S2 PI3K inhibitors suppress cell spreading mediated by *trans*-homophilic interaction of CADM1. (A) Cell spreading assay was performed with DMSO, LY294002 (1 μM), or Wortmannin (1 μM) and quantified as indicated in Fig. 1. The surface area was normalized to that of cells on IgG with DMSO, and the relative value to cells on CADM1-EC-Fc with DMSO is shown. (B, C and D) Representative images of spreading assay shown in Fig. 2A (B), Fig. 2B (C) and Fig. 3C (D). Cells stained with phalloidin are shown. Bars: 50 μm.
(TIF)

Figure S3 Localization of MPP3, Dlg, and p85 in Caco-2 cells depleted CADM1. (A and B) Immunofluorescence analysis of Caco-2 cells stably expressing shNegative or shCADM1_5 using antibodies indicated on top of images. Arrowheads and arrows show colocalization and mislocalization of indicated proteins, respectively, at cell-cell contact sites. Bars: 20 μm. (C) Immunoblot analysis of Caco-2 cells expressing shNegative or shCADM1_5 with anti-CADM1 and anti-GAPDH antibodies.
(TIF)

Figure S4 Localization of GFP-Akt-PH and the components of CADM1 complex in cell spreading assay. (A) Representative images of MDCK cells transfected with GFP-Akt-PH, CADM1-WT or ΔCT, and/or siNegative or siDlg_2 and analyzed by spreading assays indicated at the left side of images. Immunofluorescence analysis was performed using antibodies against MPP3, Dlg, CADM1, and p85 as indicated. Bars: 20 μm. (B) Immunoblot analysis of MDCK cells transiently tranefected with siNegative, siDlg_1, or siDlg_2.
(TIF)

Figure S5 Schematic representation of the signaling pathways mediated by *trans*-homophilic interaction of CADM1 to cell spreading. When attached on the glass coated with CADM1-EC-Fc (upper), CADM1-expressing cells activate PI3K through MPP3 and Dlg, induce actin reorganization, and show cell spreading (lower).
(TIF)

Methods S1 Expression vectors, Cell culture and transfection, Antibodies and reagents, Immunoprecipitation and Western blotting, and Cell aggregation assay.
(DOCX)

Acknowledgments

The authors express their gratitude to Dr. T. Akaike, Tokyo Institute of Technology for the pcDNA3.1-IgG-Fc vector.

Author Contributions

Conceived and designed the experiments: SM MSY YM. Performed the experiments: SM MSY TM. Analyzed the data: SM MSY. Wrote the paper: SM MSY YM.

References

1. Juliano RL (2002) Signal transduction by cell adhesion receptors and the cytoskeleton: functions of integrins, cadherins, selectins, and immunoglobulin-superfamily members. Annu Rev Pharmacol Toxicol 42: 283–323.
2. Cavallaro U, Christofori G (2004) Cell adhesion and signalling by cadherins and Ig-CAMs in cancer. Nat Rev Cancer 4: 118–132.
3. Doherty P, Walsh FS (1996) CAM-FGF receptor interactions: a model for axonal growth. Mol Cell Neurosci 8: 99–111.
4. Bienz M, Clevers H (2000) Linking colorectal cancer to Wnt signaling. Cell 103: 311–320.